Synchrotron tomography of a stem-lizard elucidates early squamate anatomy

Mateusz Tałanda[1,2]*, Vincent Fernandez[3,4], Elsa Panciroli[5,6,7], Susan E. Evans[2], Roger J. Benson[5]*

[1]University of Warsaw, Faculty of Biology, Biological and Chemical Research Centre, Institute of Evolutionary Biology, Warsaw, Poland

[2]Centre for Integrative Anatomy, Department of Cell and Developmental Biology, University College London, London, UK

[3]ESRF, The European Synchrotron, Grenoble, France

[4]Core Research Laboratories, The Natural History Museum, London SW7 5BD, UK

[5]Department of Earth Sciences, University of Oxford, South Parks Road, Oxford OXI 3AN, UK

[6]Natural Sciences Department, National Museums Scotland, Chambers Street, Edinburgh, UK

[7]Oxford University Museum of Natural History, Parks Road, Oxford, UK

*Correspondence: m.talanda@uw.edu.pl, roger.benson@earth.ox.ac.uk

Squamates (lizards and snakes) include more than 10,000 living species, descended from an ancestor that diverged more than 240 million years ago from that of their closest living relative, *Sphenodon*. However, a deficiency of fossil evidence [1–7], combined with serious conflicts between molecular and morphological accounts of squamate phylogeny [8–13] (but see [14]), has caused uncertainty about the origins and evolutionary assembly of squamate anatomy. We report the near-complete skeleton of a stem-squamate *Bellairsia gracilis* from the Middle Jurassic of Scotland, documented using high-resolution, synchrotron, phase-contrast tomography. *Bellairsia* shares numerous features of the crown-group, including traits related to cranial kinesis, an important functional feature of many extant squamates, and those of the braincase and shoulder girdle. Alongside these derived traits, *Bellairsia* also retains inferred ancestral features including a pterygoid-vomer contact and the presence of both cervical and dorsal intercentra. Phylogenetic analyses return strong support for *Bellairsia* as a stem-squamate, suggesting that several features that it shares with extant gekkotans are plesiomorphies, consistent with the molecular phylogenetic hypothesis that gekkotans are early-diverging squamates. We also provide confident support of stem-squamate affinities for the enigmatic *Oculudentavis*. Our findings indicate that squamate-like functional features of the suspensorium, braincase and shoulder girdle, preceded the origin of their palatal and vertebral traits, and indicate the presence of advanced stem-squamates as persistent components of terrestrial assemblages up to at least the mid Cretaceous.

Squamates are among the most speciose of extant vertebrate radiations and are characterised by numerous derived features of both the skull and postcranium. They diversified from an ancestor possessing some or all of these traits, giving rise to taxa as morphologically disparate as snakes, amphisbaenians, chameleons, geckos, and the extinct marine mosasaurs. However, definite stem-squamate fossils representing the early history of the group have until now been rare or absent, spanning from their inferred time of origin in the early Middle Triassic (240 million years ago based on fossils, and older from molecular clock studies [3,15]), up to the late Early Cretaceous [11,16,17]. This lack of fossil data may explain deep uncertainties regarding the ancestral anatomical states of the squamate crown-group, as evident from conflicts between phylogenetic hypotheses of the relationships among major groups [1,2]. In particular, morphological hypotheses place iguanians as the sister to all other squamates,

implying that traits such as presence of a choanal fossa on the palatine, lack of vomer-pterygoid contact, vertebral procoely, and loss of distal tarsal 2 are potentially plesiomorphic for squamates [11]. In contrast, molecular phylogenetic hypotheses have consistently resolved iguanians as being deeply-nested, with snakes (Serpentes) and anguimorphs, instead finding gekkotans and/or dibamids as the earliest-diverging crown squamates [10,12,13]. Morphological evidence for this has been scarce [8,11] (but see [14]).

We report a near-complete (~70%) skeleton (Fig. 1, Extended Data Fig. 1) of the tiny, Middle Jurassic squamate-like taxon *Bellairsia gracilis* from the Bathonian Kilmaluag Formation of the Elgol site of special scientific interest (Elgol SSSI), Isle of Skye, Scotland [18]: NMS G.2022.1.1 (see SI for taxonomy and locality data). *Bellairsia gracilis* was previously known only from more fragmentary, microvertebrate remains that, along with other microvertebrate remains from the Middle Jurassic (Bathonian) of the UK [18–22] share features with crown-squamates [21]. However, the disassociated nature of these specimens has limited their usefulness for understanding early squamate evolution. Here, we use high-resolution laboratory X-ray micro-CT and phase contrast synchrotron X-ray micro-CT of the new specimen to visualise the whole skeleton of *Bellairsia*, excluding the mid-distal tail and the anterior portion of the snout, which are not preserved. Phylogenetic analysis provides strong evidence that *Bellairsia* is a stem-squamate, shedding light on the origins of squamate crown-group anatomy. We also find evidence of stem-squamate affinities for some other fossil species, indicating that stem-squamates persisted in terrestrial ecosystems up to at least the mid Cretaceous (Albian-Cenomanian).

Description

The specimen is dorsoventrally compressed but preserves most of the skull and skeleton in partial articulation (Fig. 1). Based on the preserved portion of skeleton we estimate the snout-pelvis length (roughly equivalent to snout-vent length in living lizards) as roughly 60-70 mm. The specimen appears to be close to adult size, but was probably not fully mature, based on the co-ossification of the scapula and coracoid, the near fusion of the pelvic elements and of the astragalus and calcaneum in the ankle, and the ossification of the long-bone epiphyses, although slight displacements suggest these epiphyses were not yet completely fused to the diaphyses.

The skull roof is displaced ventrolaterally relative to the basicranium, due to compression, and most of the snout is missing (premaxillae, septomaxillae, vomers, anterior maxillae). The preserved part of the skull roof (complete parietal and frontal, posterior part of nasal) is about 10 mm long. The orbits are relatively large and, consequently, the frontal is only 2.2 mm wide at its narrowest point. The upper and lower temporal fenestrae were open.

The nasals are damaged but may be fused. The unpaired frontal is not sculptured, but the posterior portion bears a shallow Y-shaped groove that may mark the original positions of large head scales (scutes). The frontal is of similar width through the anterior two-thirds, with little orbital emargination, suggesting the eyes were not enlarged. Ventrally, the frontal bears shallow subolfactory ridges. Anterior to the orbit, the prefrontal facet occupies more than one third of the frontal length but, unusually, there is no posterolateral facet for the postfrontal. At the fronto-parietal suture, the straight mid-frontal margin bears a narrow shelf that underlaps the parietal, whereas the posterolateral frontal processes overlap the parietal. Together, these features create a firm, akinetic, articulation. The domed parietal is preserved in two parts but is broken rather than paired. There is no trace of a parietal foramen, and the posterior margin is extended into a median postparietal projection.

The prefrontals form the entire anterior margin of the orbit and each tapers posteroventrally to contact the jugal, lacrimal, maxilla, and ectopterygoid. The lacrimal duct lay between the lacrimal and prefrontal. The small postfrontals are dorsoventrally flattened and quadriradiate (Extended Data Fig. 2). Their medial surface is smooth, with no obvious facets for the frontal or parietal. This suggests the contact between the postfrontal and skull roof was ligamentous, an interpretation consistent with the lack of a postfrontal facet on the frontal. A shallow facet on the lateral margin may be for a postorbital, but this element has not been confidently identified. The jugal is a large, robust bone that bears a very short posterior process. The tapering postorbital process also appears short and may not have been in bony contact with the postorbital. It is therefore possible that the postorbital bar was incomplete. A flattened, rod-like element near the top of the quadrate may be part of a squamosal.

The quadrates were displaced during compaction. The left one is better-preserved. It bears a deep dorsal squamosal notch and a well-developed, but shallow, lateral conch. Ventromedially, there is a small anteromedially directed pterygoid lappet, but no medial wing (Extended Data Fig. 3).

The palate is represented by the palatines and pterygoids, with the latter completely separating the former in the midline. The palatine lacks both teeth and a choanal groove. The pterygoids met the vomers anteriorly but were not themselves in contact. A small oval group of denticles lies in the centre of each bone and the quadrate process bears an oval dorsal pit (fossa columellae) for the epipterygoid (Extended Data Figs 2, 3).

In the braincase the basisphenoid has long slender basipterygoid processes with expanded distal ends (Extended Data Fig. 3). These processes are pierced at their base by a short vidian canal. A foramen for cranial nerve VI (abducens) perforates a low crista sellaris. The basioccipital basal tubera are well developed. The lateral opening of the recessus scalae tympani is visible next to the right basal tuber. It forms an occipital recess, bordered posteroventrally by a crista tuberalis that separates it from the vagus foramen. The exoccipital is pierced by hypoglossal foramina and seems firmly fused to the basioccipital. Whether it was also fused to the opisthotic is unclear due to compression.

Only the posterior parts of each dentary are preserved in NMS G.2022.1.1. However, other specimens (NHMUK PV R12678; NMS G.2019.34.1; NMS G1992.47.10 [Extended Data Fig. 4]) give a dentary tooth count of around 25. The teeth are supported by a well-developed subdental shelf that bears a splenial facet above an open Meckelian fossa. The preserved portion of the dentary has subparallel dorsal and ventral margins and forks posteriorly into two processes of similar length. Of the post-dentary elements, the right coronoid bears a well-developed dorsal (coronoid) process but no labial process. The surangular and angular form the dorsal and posteroventral parts of the mandible respectively, and there is a well-developed retroarticular process with a sharp lateral crest.

The tooth implantation is pleurodont. The teeth are unworn, and the crowns are labiolingually flattened with apicobasally-oriented anterior and posterior grooves on their lingual surfaces. The tooth rows show lingual replacement pits and gaps for unimplanted teeth.

There are 24 deeply amphicoelous and notochordal presacral vertebrae, with free intercentra persisting intervertebrally along the whole presacral column (Fig. 2). Post-axial cervical

vertebrae are short and bear a mid-ventral sagittal ridge and well-developed neural spines. It is uncertain which cervical vertebra bore the first pair of ribs, but they were certainly present from the fourth cervical. All dorsal vertebrae bear ribs. Two short sacral vertebrae are crushed against the pelvis. Most of the tail was lost.

The scapulocoracoid has a shallow scapulocoracoid embayment, as well as deep scapula and primary coracoid emarginations (Extended Data Fig. 5). The ilium, pubis, and ischium are also conjoined, albeit with some of the suture lines still visible (Fig. 3). The hind limb is much longer than the forelimb (~ 32.2 mm vs 24.5 mm), and the pes forms the longest segment. Both femoral epiphyses are slightly dislocated suggesting that they were not fully attached. The tibial epiphysis bears a slight distal concavity suggesting the presence of a distal notch. The astragalus and calcaneum are fused. Distal to them are a large trapezoidal distal tarsal (DT) IV; a much smaller DT III; and a small irregular DT II (Fig. 3). Metatarsal (Mt) I-IV are elongated and slender, whereas the hooked Mt V is very short (~2 mm), with well-developed medial and lateral plantar tubercles (Fig. 3). The pedal phalangeal formula is 2-3-4-5-4.

Phylogenetic results

Phylogenetic analyses of a modified version of the matrix of [14,23,24] recovers strong support (posterior probability [pp] = 1.0) for *Bellairsia gracilis* as a stem-squamate, as part of a sister-clade to the squamate crown-group that also includes the mid-Cretaceous taxa *Huehuecuetzpalli mixtecus* (Albian, Mexico) and *Oculudentavis naga* (Cenomanian, Myanmar) (Fig. 4). Their position close to the crown of Squamata is supported by 23 synapomorphies, including the absence of quadratojugals and gastralia, fusion of parietals, and an anterolaterally directed transverse flange of the pterygoid (see SI for complete character optimisations). Stem-squamate affinities were previously recognised for *Huehuecuetzpalli* [11,14,16,25], but our expanded analysis resolves previous uncertainties regarding *Oculudentavis*. *Oculudentavis* was initially described as a bird[26] before recognition of squamate-like features of the braincase, suspensorium and pectoral girdle[27,28], with uncertain affinities as either a stem- or crown-squamate depending on analysis[27,28].

Although we are confident that *Bellairsia*, *Huehuecuetzpalli* and *Oculudentavis* are stem-squamates, the hypothesis that they form a clade is less well-supported. Seven synapomorphies are inferred (see SI). However, four of these are not known due to missing data in *Huehuecuetzpalli* and only one step is required to remove this taxon from the grouping in parsimony analysis. Support for the position of *Bellairsia* and *Oculudentavis naga* in this clade is stronger than for *Huehuecuetzpalli* as the two require at least five more steps to move them into a different place in the tree (and see SI for shared character states of *Bellairsia* and *Oculudentavis*). *Bellairsia* and *Oculudentavis* could potentially represent an unrecognized clade of stem-squamates. However, they are separated by a long period of geological time, and future finds and analyses will test their phylogenetic relationships.

Crown squamates are supported by 13 synapomorphies that are absent in *Bellairsia*, including closure of the notochordal canal in adults[29] (except in gekkotans) and the presence of a styloid process on the radius (for details of the characters supporting these nodes, see SI). In our main analysis (Extended Data Figure 7B), *Hongshanxi* from the Middle/Late Jurassic (late Callovian or early Oxfordian) of China[30] is found in a polytomy at the base of the squamate crown-group and therefore is also a possible stem-squamate, but could alternatively be a member of the crown more advanced than Gekkota, given its procoelous vertebrae and temporal osteoderms[30].

Discussion

Near-complete skeletal preservation of the stem-squamate *Bellairsia gracilis* provides new insights into the evolutionary assembly of squamate anatomy. The anatomy of *Bellairsia* may have particular relevance to inferring character state transitions preceding squamate origins, given its early stratigraphic occurrence (~167 Ma), pre-dating the occurrence of *Huehuecuetzpalli*[17], from the Early Cretaceous (Albian) of Mexico [16,17], by more than 60 million years, and therefore with less time for the independent evolution of derived states. Previously, *Huehuecuetzpalli mixtecus* was the only taxon to be confidently identified as a stem-squamate [11,14,24,28] (but see [31] who placed it as a stem-iguanian), but has not been subject to high-resolution CT, and occurred 105 million years ago, approximately 100 million years after the inferred origin of the squamate crown-group in the Late Triassic or Early Jurassic [1,3,14]. Moreover, it possessed various specialisations, including posteriorly extended narial openings, an anteriorly placed parietal foramen, and hypothesised bipedal locomotion[17,25].

Bellairsia was original attributed to Scincomorpha[21], a grouping of scincoid and lacertoid lizards[8,11] that is not supported by molecular phylogenies[9,10,12,13]. However, this was based mainly on jaw and dental characters now known to be more widely distributed. The new specimen is considerably more complete and shows that *Bellairsia* possesses a mosaic of primitive (ancestral) and derived traits, indicating that squamate-like functional features of the suspensorium, braincase and shoulder girdle preceded the origin of their palatal and vertebral traits. *Bellairsia* (like *Oculudentavis*) shares numerous derived features with crown-squamates, including the divided metotic fissure, enclosed vidian canal, fully pleurodont teeth, absence of gastralia, and emarginated scapulocoracoid. The quadrate was streptostylic, possibly enabling anteroposterior translational movements during feeding [32], and there was a synovial joint between the epipterygoid and palate, as indicated by the fossa columellae on the pterygoid of *Bellairsia*. These observations suggest that key aspects of squamate skull function first appeared on their stem-lineage. Nevertheless, *Bellairsia* also lacks some of the derived cranial traits that are present in most squamates. For example, *Bellairsia* lacks the choanal groove found on the palatine of most crown-taxa. It also has a contact between the pterygoid and vomer, which is absent in most crown squamates due to expansion of the palatines, possibly to reduce the strain between the muzzle unit and the rest of the skull [33]. The retention of a pterygoid-vomer contact, in combination with the firm frontal-parietal suture, suggests that mesokinesis, an important functional feature of many crown-squamates, was not yet developed in *Bellairsia*.

The postcranial skeleton of *Bellairsia* also shows some apparently primitive features. The ankle retains three distal tarsals and MTV is hooked, as seen in all crown-lepidosaurs, but is not inflected, unlike that of most crown squamates. Moreover, *Bellairsia* has amphicoelous, notochordal vertebrae with intercentra present along the presacral series, whereas most extant lizards have procoelous vertebrae with intercentra restricted to the neck. Only geckos (procoelous and amphicoelous) and xantusiids have intercentra on the dorsal vertebrae [29].

The anatomy of *Bellairsia* may also help resolve questions regarding the primitive morphology of squamates and provide morphological support for gekkotans as early-diverging squamates. Classic morphological hypotheses of squamate evolution proposed Iguania as the sister to ‘Scleroglossa’, comprising all other extant squamate lineages, including gekkotans [8,11,31]. This hypothesis has been repeatedly challenged by molecular phylogenetics, which return a deeply-nested position of Iguania, and find support for Gekkota and/or Dibamidae as the sister to all other extant squamate lineages[9,10,34,35]. However, morphological evidence for this has been limited, or strongly contradictory (e.g. [11]; but see[14]), and represents one of the most contentious uncertainties of vertebrate phylogenetics (e.g. [12]).

Bellairsia shares several features with gekkotans, including the lack of a parietal foramen (also in dibamids, teiids, gymnophthalmids, *Heloderma*, *Lanthanotus*, variable in scincoids[32]), intercentra present between all presacral vertebrae (also in xantusiids [29]), and amphicoelous vertebrae. We find strong evidence that these traits are plesiomorphic for the squamate crown-group rather than being derived traits of a *Bellairsia*+Gekkota clade: the phylogenetic hypothesis that *Bellairsia* is the sister to Gekkota requires 15 additional steps and the hypothesis that *Bellairsia* is sister to Gekkota+*Dibamus* or to *Eichstaettisaurus*+(*Dibamus*+Gekkota) requires 10 additional steps. Therefore, key aspects that differentiate gekkotans from most other extant squamates may result from the retention of primitive features in Gekkota, and not from independent specialisation.

Identification of *Bellairsia* as a stem-squamate provides support for the transitional nature of the Middle Jurassic tetrapod assemblages, which retained components of archaic lineages alongside early members of the living crown groups, not only among squamates and other lepidosaurs, but also in mammals and amphibians. For example, *Bellairsia* co-occurs at both Kirtlington and the Elgol SSSI alongside the stem-lepidosaur *Marmoretta*, stem-mammals such as docodonts, and stem-salamanders such as *Marmorerpeton* [18,23,36–39]. Our phylogenetic analysis indicates that some of these stem-squamate elements persisted longer still, and with greater diversity than previously recognised. If our placement of *Huehuecuetzpalli* and *Oculudentavis* is confirmed, then stem-squamate lineages persisted on different continents alongside crown-squamates at least until the mid-Cretaceous (Albian-Cenomanian).

Taken together, our results provide evidence of the anatomical transformations involved in the origins of squamate anatomy. This early diversification phase gave rise not only to important living groups within the crown, but also to other lineages, including crownward stem-squamates, that are now extinct. The transition to more modern-like assemblages took place gradually over more than 100 million years across a global arena. The acquisition of the derived traits that characterise crown-squamates and led to the evolution of groups as diverse as snakes, geckos, chameleons and mosasaurs occurred in a mosaic fashion which we are only now beginning to understand.

References

1. Evans, S. E. At the feet of the dinosaurs: the early history and radiation of lizards. *Biol. Rev. Camb. Philos. Soc.* **78**, 513–551 (2003).
2. Evans, S. E. & Jones, M. E. H. The origin, early history and diversification of lepidosauromorph reptiles. *New Asp. Mesozoic Biodivers.* 27–44 (2010). doi:10.1007/978-3-642-10311-7
3. Jones, M. E. H. *et al.* Integration of molecules and new fossils supports a Triassic origin for Lepidosauria (lizards, snakes, and tuatara). *BMC Evol. Biol.* **13**, 208 (2013).
4. Cavicchini, I., Zaher, M. & Benton, M. J. An enigmatic neodiapsid reptile from the Middle Triassic of England. *J. Vertebr. Paleontol.* **40**, (2020).
5. Sues, H. D. & Kligman, B. T. A new lizard-like reptile from the Upper Triassic (Carnian) of Virginia and the Triassic record of Lepidosauromorpha (Diapsida, Sauria). *J. Vertebr. Paleontol.* **40**, 1–11 (2020).
6. Skutschas, P. P. *et al.* A lepidosauromorph specimen from the Middle Jurassic (Bathonian) Moskvoretskaya Formation of the Moscow Region, Russia. *Hist. Biol.* **00**, 1–5 (2021).
7. Sobral, G., Simões, T. R. & Schoch, R. R. A tiny new Middle Triassic stem-lepidosauromorph from Germany: implications for the early evolution of lepidosauromorphs and the Vellberg fauna. *Sci. Rep.* **10**, (2020).

8. Estes, R., De Queiroz, K. & Gauthier, J. Phylogenetic relationships within Squamata. in *Essays Commemorating Charles L. Camp. Phylogenetic Relationships of the Lizard Families* (eds. Estes, R. & Pregill, G.) 119–281 (Stanford University Press, 1988).
9. Townsend, T. M., Larson, A., Louis, E. & Macey, J. R. Molecular phylogenetics of squamata: the position of snakes, amphisbaenians, and dibamids, and the root of the squamate tree. *Syst. Biol.* **53**, 735–57 (2004).
10. Vidal, N. & Hedges, S. B. The phylogeny of squamate reptiles (lizards, snakes, and amphisbaenians) inferred from nine nuclear protein-coding genes. *Comptes Rendus - Biol.* **328**, 1000–1008 (2005).
11. Gauthier, J., Kearney, M., Maisano, J. A., Rieppel, O. & Behlke, A. D. B. Assembling the squamate Tree of Life: perspectives from the phenotype and the fossil record. *Bull. Peabody Museum Nat. Hist.* **53**, 3–308 (2012).
12. Losos, J. B., Hillis, D. M. & Greene, H. W. Who speaks with a forked tongue? *Science* **338**, 1428–1429 (2012).
13. Burbrink, F. T. *et al.* Interrogating genomic-scale data for Squamata (lizards, snakes, and amphisbaenians) shows no support for key traditional morphological relationships. *Syst. Biol* **69**, 502–520 (2020).
14. Simões, T. R. *et al.* The origin of squamates revealed by a Middle Triassic lizard from the Italian Alps. *Nature* **557**, 706–709 (2018).
15. Pyron, R. A. Novel approaches for phylogenetic inference from morphological data and total-evidence dating in squamate reptiles (lizards, snakes, and amphisbaenians). *Syst. Biol.* **66**, 38–56 (2017).
16. Reynoso, V. *Huehuecuetzpalli mixtecus* gen. et sp. nov: a basal squamate (Reptilia) from the Early Cretaceous of Tepexi de Rodríguez, central México. *Philos. Trans. R. Soc. B Biol. Sci.* **353**, 477–500 (1998).
17. Villaseñor-Amador, D., Suárez, N. X. & Cruz, J. A. Bipedalism in Mexican Albian lizard (Squamata) and the locomotion type in other Cretaceous lizards. *J. South Am. Earth Sci.* **109**, 103299 (2021).
18. Panciroli, E. *et al.* Diverse vertebrate assemblage of the Kilmaluag Formation (Bathonian, Middle Jurassic) of Skye, Scotland. *Earth Environ. Sci. Trans. R. Soc. Edinburgh* **111**, 135–156 (2020).
19. Evans, S. E. Jurassic lizard assemblages. *Rev. Paléobiologie, Genève* **7**, 55–65 (1993).
20. Evans, S. E. A new anguimorph lizard from the Jurassic and Lower Cretaceous of England. *Palaeontology* **37**, 33–49 (1994).
21. Evans, S. E. Crown group lizards (Reptilia, Squamata) from the Middle Jurassic of the British Isles. *Palaeontogr. Abteilung A Palaozoologie - Stratigr.* **250**, 123–154 (1998).
22. Waldman, M. & Evans, S. E. Lepidosauromorph reptiles from the Middle Jurassic of Skye. *Zool. J. Linn. Soc.* **112**, 135–150 (1994).
23. Griffiths, E. F., Ford, D. P., Benson, R. B. J. & Evans, S. E. New information on the Jurassic lepidosauromorph *Marmoretta oxoniensis*. *Pap. Palaeontol.* **7**, 2255–2278 (2021).
24. Ford, D. P., Evans, S. E., Choiniere, J. N., Fernandez, V. & Benson, R. B. J. A reassessment of the enigmatic diapsid *Paliguana whitei* and the early history of Lepidosauromorpha. *Proc. R. Soc. B Biol. Sci.* **288**, 20211084 (2021).
25. Reynoso, V.-H. & Cruz, J. A. Mesozoic lepidosauromorphs of Mexico: a review and discussion of taxonomic assignments. in *Dinosaurs and Other Reptiles from the Mesozoic of Mexico* (eds. Rivera-Sylva, H. E., Carpenter, K. & Frey, E.) 4–44 (Indiana University Press, 2014).
26. Xing, L. *et al.* Hummingbird-sized dinosaur from the Cretaceous period of Myanmar. *Nature* **579**, 245–249 (2020).

27. Li, Z.-H. *et al.* Reanalysis of *Oculudentavis* shows it is a lizard. *Vertebr. Palasiat.* **59**, 95–105 (2020).
28. Bolet, A. *et al.* Unusual morphology in the mid-Cretaceous lizard *Oculudentavis*. *Curr. Biol.* **31**, 3303–3314 (2021).
29. Hoffstetter, R. & Gasc, J.-P. Vertebrae and ribs of modern reptiles. *Biol. Reptil.* **1**, 201–310 (1969).
30. Dong, L., Wang, Y., Mou, L., Zhang, G. & Evans, S. E. A new Jurassic lizard from China. *Geodiversitas* **41**, 623–641 (2019).
31. Conrad, J. L. Phylogeny and systematics of Squamata (Reptilia) based on morphology. *Bull. Am. Museum Nat. Hist.* **310**, 1–182 (2008).
32. Evans, S. E. The skull of lizards and Tuatara. *Biol. Reptil.* **20**, 1–347 (2008).
33. Moazen, M., Curtis, N., O'Higgins, P., Evans, S. E. & Fagan, M. J. Biomechanical assessment of evolutionary changes in the lepidosaurian skull. *Proc. Natl. Acad. Sci. U. S. A.* **106**, 8273–8277 (2009).
34. Vidal, N. & Hedges, S. B. The molecular evolutionary tree of lizards, snakes, and amphisbaenians. *Comptes Rendus - Biol.* **332**, 129–139 (2009).
35. Wiens, J. J. *et al.* Resolving the phylogeny of lizards and snakes (Squamata) with extensive sampling of genes and species. *Biol. Lett.* 1043–1046 (2012). doi:10.1098/rsbl.2012.0703
36. Panciroli, E. *et al.* Postcrania of *Borealestes* (Mammaliformes, Docodonta) and the emergence of ecomorphological diversity in early mammals. *Palaeontology* **65**, 1–36 (2022).
37. Panciroli, E., Benson, R. B. J. & Luo, Z. X. The mandible and dentition of *Borealestes serendipitus* (Docodonta) from the Middle Jurassic of Skye, Scotland. *J. Vertebr. Paleontol.* **39**, (2019).
38. Caldwell, M. W., Nydam, R. L., Palci, A. & Apesteguía, S. The oldest known snakes from the Middle Jurassic-Lower Cretaceous provide insights on snake evolution. *Nat. Commun.* **6**, 5996 (2015).
39. Evans, S. E. & Waldman, M. Small reptiles and amphibians from the Middle Jurassic of Skye, Scotland. *Museum North. Arizona Bull.* **60**, 219–226 (1996).

Methods

Phylogenetic analysis. We evaluated the affinities *of Bellairsia gracilis* by Bayesian phylogenetic analysis of two datasets: (Dataset 1) An amended version of the morphological character matrix of [23,24], which was originally modified from [14] and is our preferred dataset due to extensive sampling of relevant outgroups, and (Dataset 2) the matrix of [28], which was originally modified from [11]. Our main analyses use a molecular backbone to constrain the relationships of extant squamates (Extended Data Fig. 6), but we also ran minimally-constrained analyses, in which we only specified the monophyly of extant squamates relative to *Sphenodon*. Scoring of *Bellairsia* in both datasets was based on the new Skye specimen, two additional attributed dentaries from Skye (NMS G.1992.47.10 and G.2019.34.1), and the original attributed specimens from Kirtlington in Oxfordshire[21]. Modifications of Dataset 1 (from ref. [24]) include correction of some scorings of *Fraxinisaura* and *Megachirella* based on first hand observations as well as updates to scores for the Late Jurassic *Ardeosaurus*[40], and the stem-lepidosaurs *Paliguana* (Early Triassic[24]) and *Marmoretta* (Middle Jurassic[23]). We added three Mesozoic lizards, including the recently described taxa *Hongshanxi xiei* from the Middle/Upper Jurassic of China [30] and *Oculudentavis* spp. from the mid-Cretaceous of Myanmar [28], as well as *Scandensia ciervensis* from the Early Cretaceous of Spain[41]. We also added two recently-described Triassic diapsids, *Vellbergia bartholomaei*[42] and *Taytalura*

alcoberi[43], and one new character numbered 382: metotic fissure undivided (0) or subdivided (1).

All trees from the modified matrix of [23,24] (Dataset 1) placed *Bellairsia* in a small stem-squamate clade, as the sister taxon to the Mexican Cretaceous *Huehuecuetzpalli* [16] + *Oculudentavis* [28] (Extended Data Figs 7–8), including using the full molecular backbone constraint (Extended Data Figs 7 and 8A) and when minimally constrained (Extended Data Fig. 8B), and when omitting taxa with less certain phylogenetic affinities that limit resolution of the consensus tree when included in analyses (Extended Data Fig. 7): the Early Cretaceous (Barremian) *Scandensia ciervensis*[41] from Spain and the Triassic diapsid *Vellbergia bartholomaei*[42]. *Scandensia*, for which the skull is incompletely known, grouped with *Bellairsia*, *Huehuecuetzpalli* and *Oculudentavis* on the squamate stem when included, and *Vellbergia* groups among stem-lepidosaurs, but with low posterior support as to its precise affinities (Extended Data Fig. 8). Neither taxon causes topological differences to the tree shown in Fig. 4 (based on Extended Data Fig. 7).

Analysis of the matrix of [28] (itself modified from [11]) also finds strong support for *Bellairsia* as a stem-squamate, though in a group with only *Oculudentavis*, more crownward than *Huehuecuetzpalli* (Extended Data Figs 9 and 10). This result was returned whether extant squamates were constrained to a molecular backbone (Extended Data Fig. 9), or unconstrained (other than to specify *Sphenodon* and other rhynchocephalians as an outgroup; Extended Data Fig. 10). It therefore does not conflict with the results of Dataset 1, or with our broad conclusions.

Phylogenetic inference was carried out using Bayesian inference in MrBayes 3.2.7a[44], using a FBD tree prior [45,46] and relaxed clock transition model. The ages of all OTUs were specified using a uniform distribution between their minimum and maximum possible stratigraphic ages, modified from ref [14] to reflect updated or corrected knowledge of the ages of various taxa. Analysis of Dataset 1 was run for 100 million generations, sampled every 10,000th generation, with a burn-in of 50%. The effective sample size was greater than 200 for all tested parameters and an average potential scale reduction factor was 1.01 or less on all parameters, indicating convergence. Analyses of Dataset 2 took longer before convergence and were run for 200 million generations. In addition to topology and branch lengths, our analysis return estimates of variation in rate of evolution (transition frequencies among character states). These are shown for completeness in Extended Data Figs 7–10.

Computed tomography (CT). We imaged the specimen in 3D using lab-based and synchrotron computed tomography (CT) and segmented these to produce 3D digital models of the skeleton in Avizo Lite software.

Lab-based CT scans were conducted using a Zeiss Xradia 520 Versa in the Department of Materials, University of Oxford. The whole skeleton was scanned at a voxel size of 20.10 μm, and the anterior part of the skeleton was also scanned again, at a voxel size of 11.10 μm. The left forelimb was segmented from the scan of the whole specimen. Furthermore, portions of this image volume were merged to our synchrotron data prior to segmentation of the pes. This was done to restore pedal phalanges that were lost during physical preparation of the specimen prior to synchrotron scanning.

Propagation phase contrast synchrotron X-ray micro-Computed Tomography. NMS G.2022.1.1 was characterised at the ID19 beamline of the European Synchrotron Radiation Facility (ESRF, Grenoble France) using propagation phase contrast synchrotron X-ray micro-computed tomography. Imaging of the specimens was not done on the whole block but rather on specific regions of interest determined from prior investigation using laboratory X-ray micro-computed tomography. In total, 11 regions of interest were imaged on ID19,

focussing on the skull, hind limbs and the pelvis area. All datasets were acquired with identical parameters: white beam from a wiggler 150B (gap 38 mm) filtered with 12 mm of copper; sample detector distance of 3 m; indirect detector comprising a 100 µm Ce doped Gadolinium-Gallium-Garnet scintillator, 1.5x magnification from a set of photographic lenses (Victor Hasselblad AB, Gothenburg, Sweden), a PCO.edge 4.2 USB 3 (PCO, Kelheim, Germany); the combination of the beam and indirect detector resulted in a total integrated detected energy of 134 keV and an isotropic reconstructed voxel size of 4.24 µm. Each acquisition consisted of 6000 projections of 0.1 second each (4 frames of 0.025 seconds accumulated) over a 360° rotation of the specimens. The centre of rotation of the sample manipulator was shifted laterally by a distance corresponding to 800 pixels on the detector (i.e., so-called half acquisition protocol [47], allowing to reconstruct tomograms with a diameter of 3648 pixels. The tomographic reconstruction was performed with PyHST2 [48] using the single distance phase retrieval approach [49]. Post-processing of the data included: change of the dynamic range from 32 to 16-bit, ring correction [50], cropping of the data.

Data availability

All CT data and 3D models reported in this paper are available at Morphosource for open download at www.morphosource.org/projects/00000C672. Our phylogenetic scripts, including full analytical settings, are available at http://doi.org/10.17605/OSF.IO/WHJT7.

40. Tałanda, M. An exceptionally preserved Jurassic skink suggests lizard diversification preceded fragmentation of Pangaea. *Palaeontology* **61**, 659–677 (2018).
41. Evans, S. E. & Barbadillo, L. J. An unusual lizard (Reptilia: Squamata) from the Early Cretaceous of Las Hoyas, Spain. *Zool. J. Linn. Soc*. **124**, 235-265 (1998).
42. Sobral, G., Simões, T. R. & Schoch, R. R. A tiny new Middle Triassic stem-lepidosauromorph from Germany: implications for the early evolution of lepidosauromorphs and the Vellberg fauna. *Sci. Rep*. **10**: 2273 (2020).
43. Martínez, R. N., Simões, T. R., Sobral, G. & Apesteguía, S. A Triassic stem lepidosaur illuminates the origin of lizard-like reptiles. *Nature* 597, 235-238 (2021).
44. Ronquist, F. *et al.* Mrbayes 3.2: Efficient bayesian phylogenetic inference and model choice across a large model space. *Syst. Biol.* **61**, 539–542 (2012).
45. Heath, T. A., Huelsenbeck, J. P. & Stadler, T. The fossilized birth-death process for coherent calibration of divergence-time estimates. *Proc. Natl. Acad. Sci. U. S. A.* **111**, (2014).
46. Stadler, T. Sampling-through-time in birth–death trees. *J. Theor. Biol.* **267**, 396–404 (2010).
47. Carlson, K. J. *et al.* The Endocast of MH1, *Australopithecus sediba*. *Science (80-.).* **333**, 1402–1407 (2011).
48. Mirone, A., Brun, E., Gouillart, E., Tafforeau, P. & Kieffer, J. The PyHST2 hybrid distributed code for high speed tomographic reconstruction with iterative reconstruction and a priori knowledge capabilities. *Nucl. Instruments Methods Phys. Res. Sect. B Beam Interact. with Mater. Atoms* **324**, 41–48 (2014).
49. Paganin, D., Mayo, S. C., Gureyev, T. E., Miller, P. R. & Wilkins, S. W. Simultaneous phase and amplitude extraction from a single defocused image of a homogeneous object. *J. Microsc.* **206**, 33–40 (2002).
50. Lyckegaard, A., Johnson, G. & Tafforeau, P. Correction of Ring Artifacts in X-ray Tomographic Images. *Int. J. Tomogr. Simul.* **18**, 1–9 (2011).

Figures

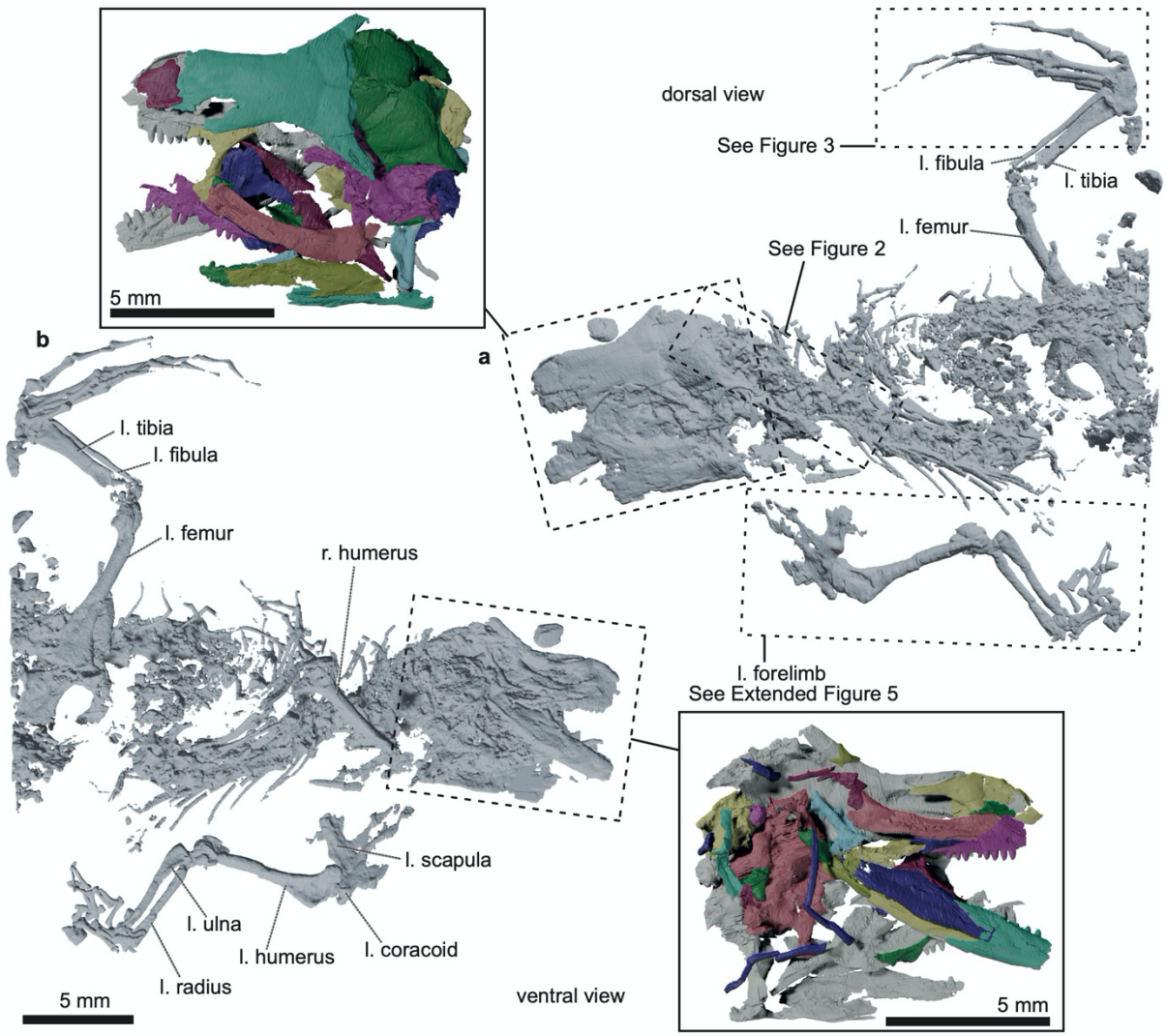

Figure 1. Skeleton of *Bellairsia gracilis* with bones digitally segmented. **a**, Preserved skeleton in dorsal view. **b**, Preserved skeleton in ventral view (see Extended Data Figs 2-4 for labelling of skull parts).

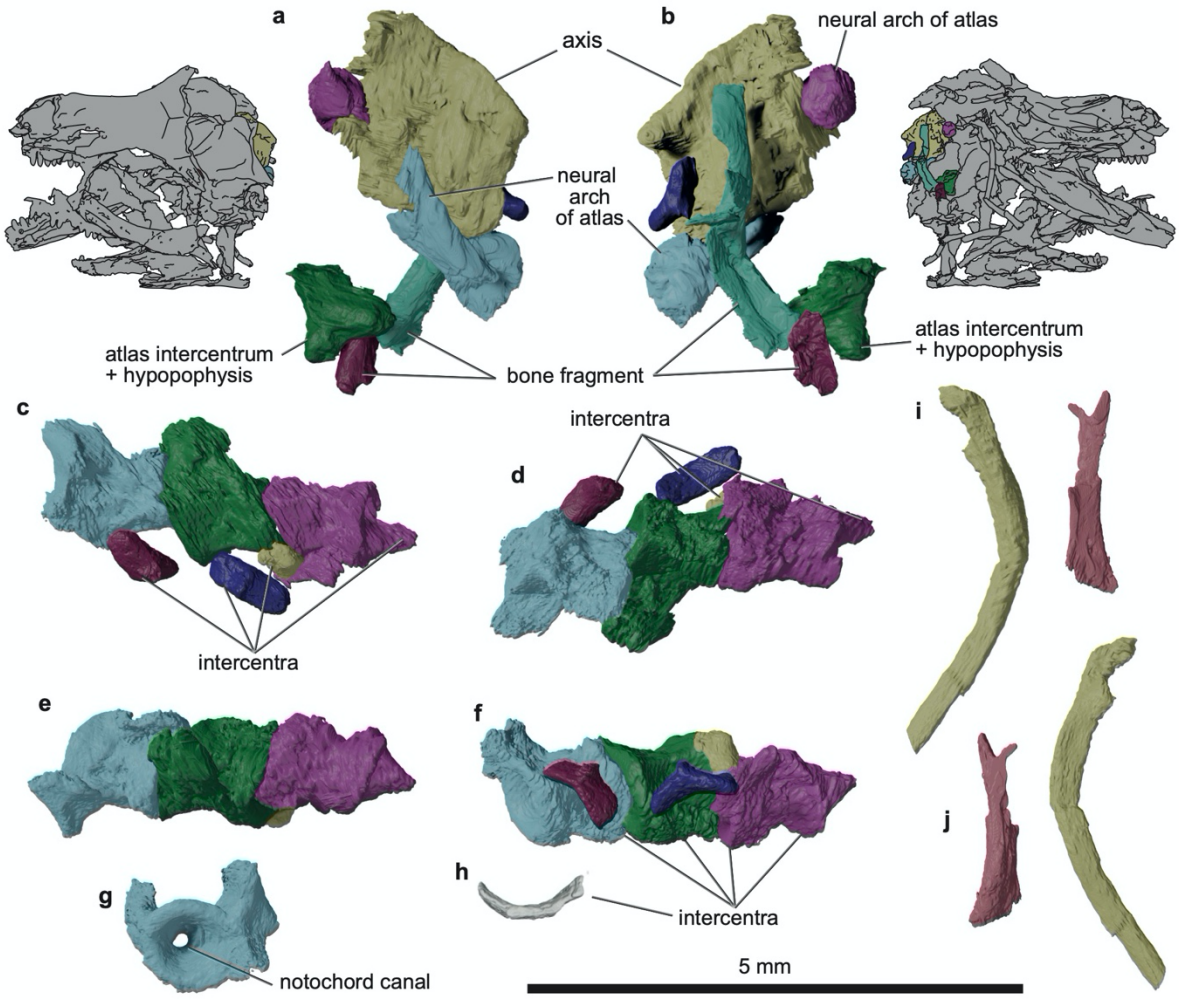

Figure 2. Cervical part of the vertebral column of *Bellairsia*. **a**, Atlas and axis in dorsal view. **b**, Atlas and axis in ventral view. **c-g**, Third, fourth, and fifth vertebrae with intercentra from various views. **h**, Intercentrum of the 22nd vertebra. **i-j**, Anterior and posterior cervical ribs.

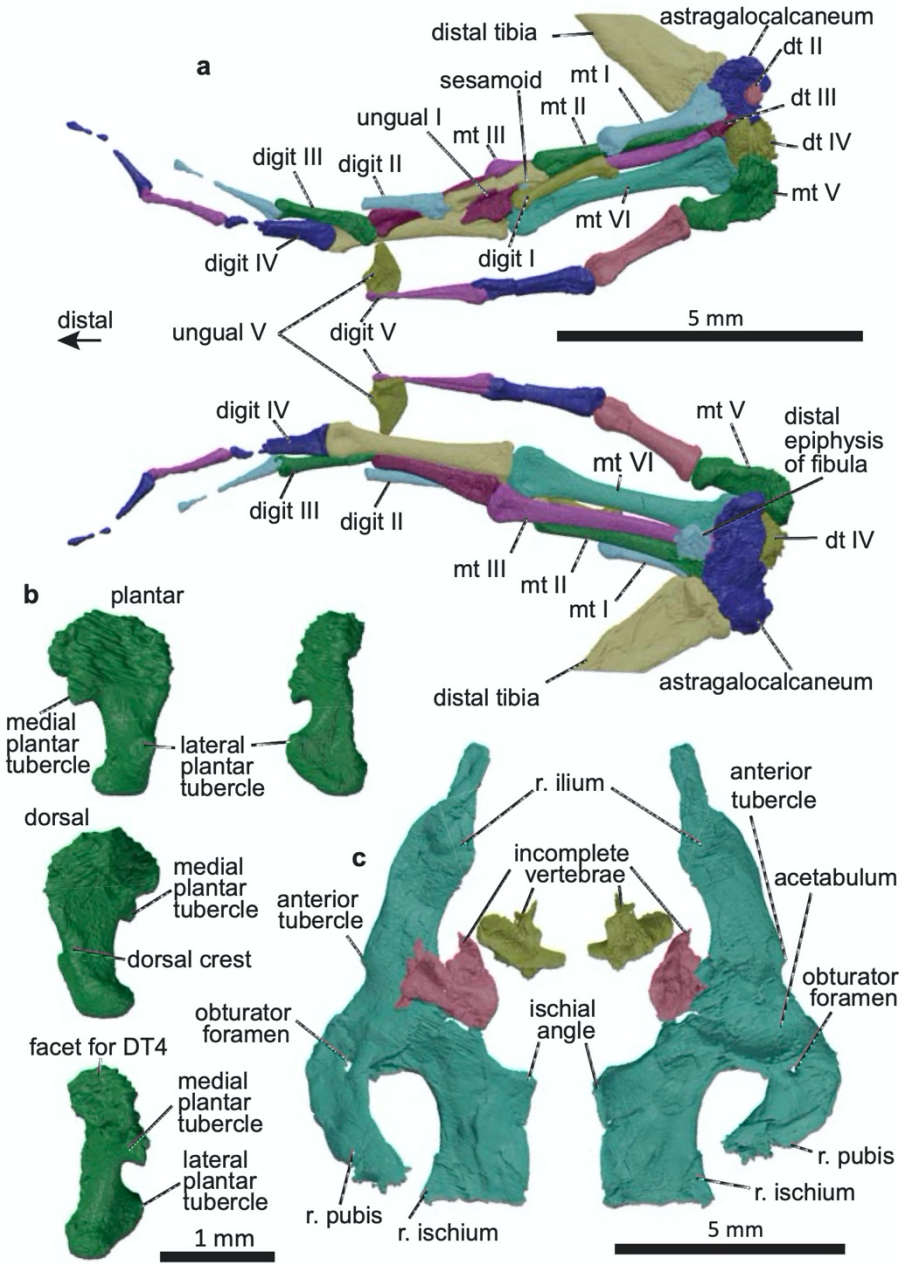

Figure 3. Right pes and pelvis of *Bellairsia*. **a**, Preserved elements of the pes in ventral and dorsal views. **b**, Fifth metatarsal in plantar, medial, dorsal, and lateral view. **c**, Pelvis in medial and lateral view.

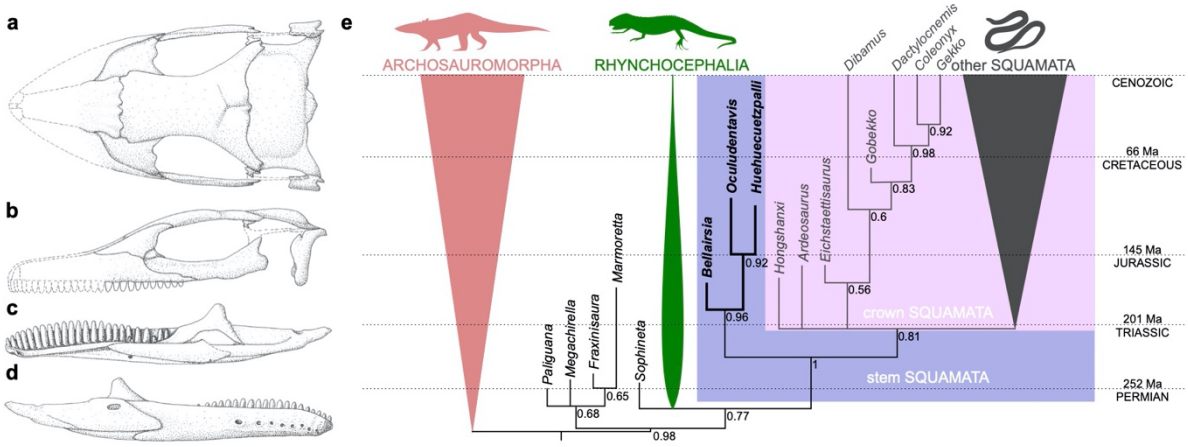

Figure 4. Linear reconstruction of the skull of *Bellairsia* and its phylogenetic position. **a**, Cranium, dorsal view. **b**, Cranium, left lateral view. **c**, Mandible, lingual view. **d**, Mandible, buccal view. **e**, Phylogenetic tree showing position of *Bellairsia* after a Bayesian analysis of the diapsid dataset (see Methods; the summary tree shown here is based on majority rule consensus of the posterior tree distribution from analysis of our modified version of the data matrix from refs [14,23,24] with molecular backbone constraint; for full tree see Extended Data Fig. 7). Numbers at nodes indicate posterior probabilities and nodes with posterior probabilities less than 0.5 are shown as unresolved. The lighter grey lines forming the snout region in A-D are speculative as these regions are not preserved, but overall snout length is based on jaw length.

Extended data figures

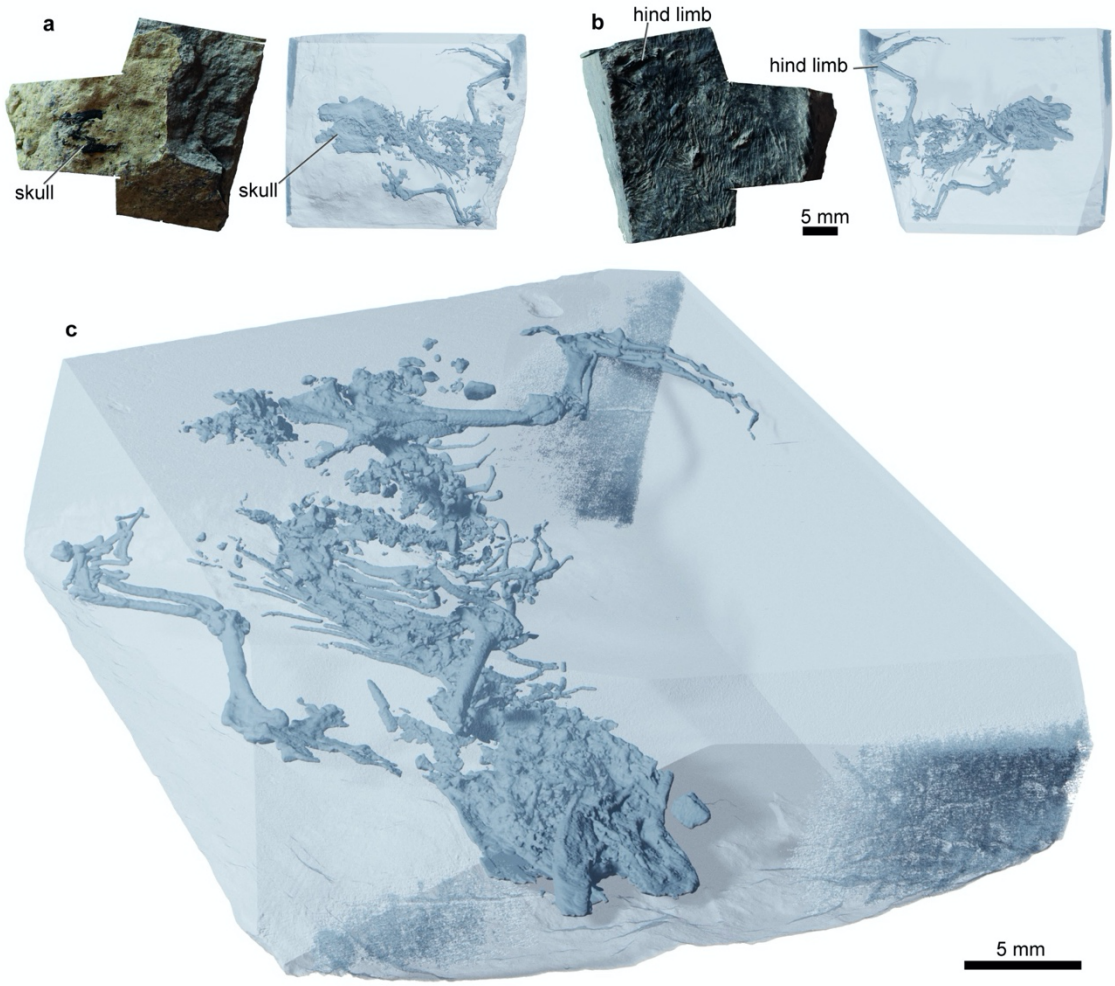

Extended Data Fig. 1. Preserved skeleton

A slab with visualized preserved skeleton of *Bellairsia gracilis* Evans, 1998 from the Middle Jurassic, Kilmaluag Formation, Skye. **a**, Dorsal. **b**, Ventral. **c**, Close-up of the visualized skeleton in the rock from anteroventral view.

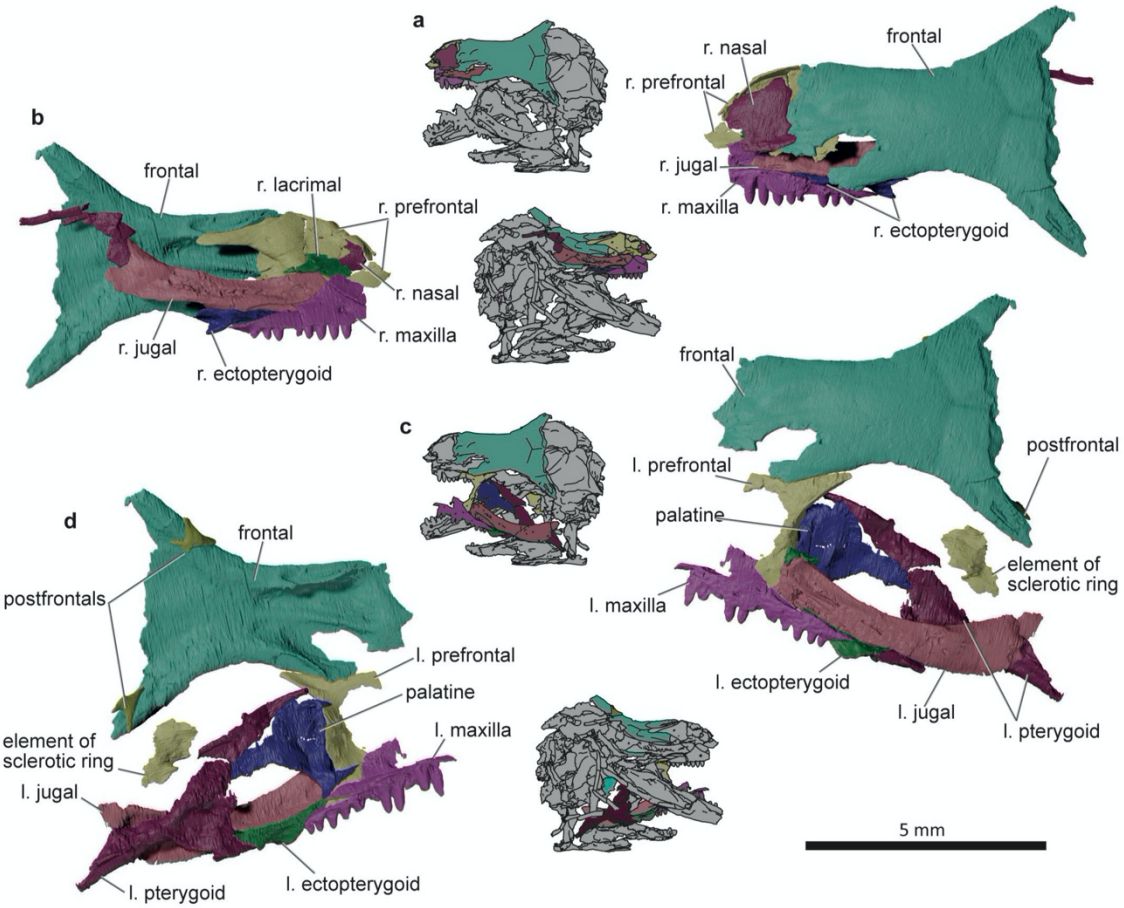

Extended Data Fig. 2. Orbital bones

Bones surrounding the orbit of *Bellairsia*. **a**, Right orbit in dorsal view. **b**, Right orbit in ventral view. **c**, Left orbit in dorsal view. **d**, Left orbit in ventral view.

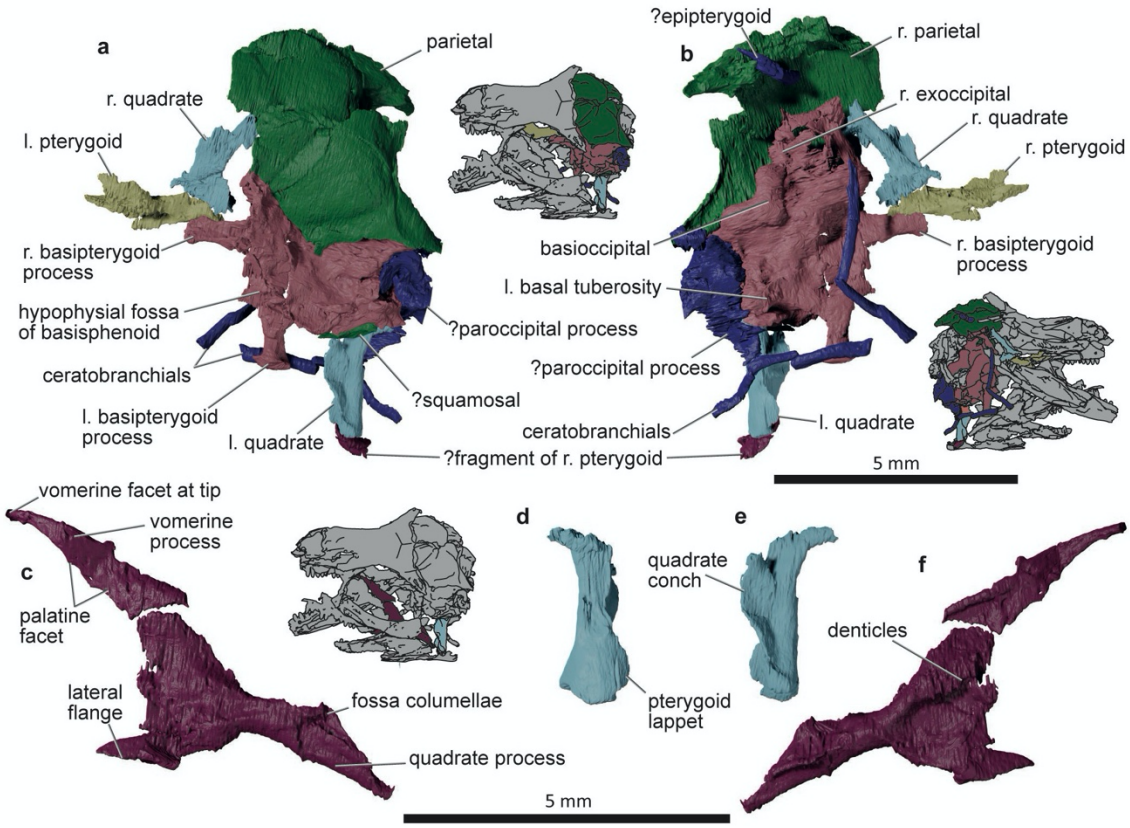

Extended Data Fig. 3. Posterior skull

Posterior part of the skull of *Bellairsia*. **a**, Dorsal view. **b**, Ventral view.

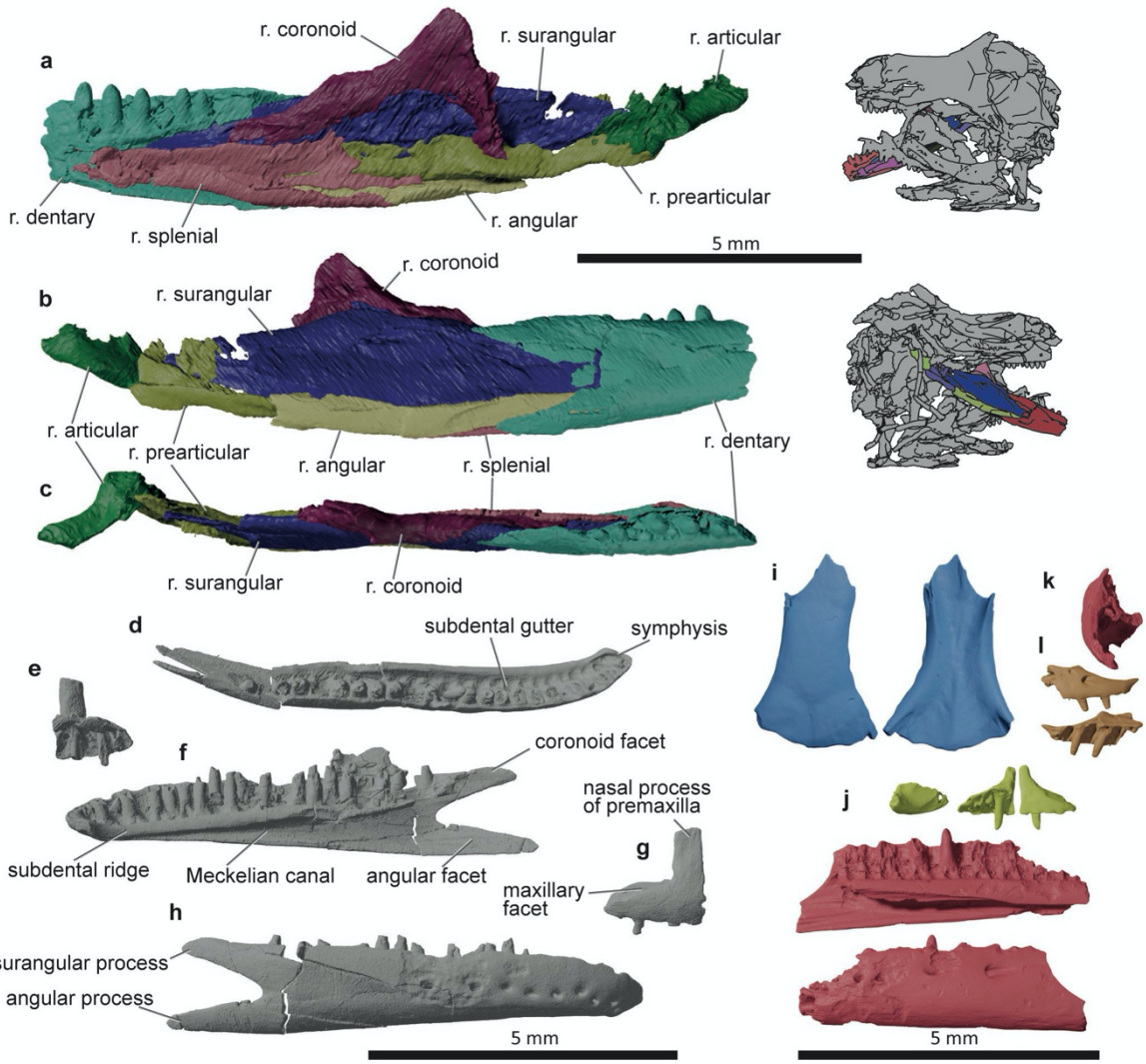

Extended Data Fig. 4. Mandible

Right mandible (ELGOL2016 021), dentary and premaxilla (NMS G1992.47.10) from Kilmaluag Formation, Skye; frontal, left premaxilla, left dentary, maxilla from Kirtlington. **a**, ELGOL2016 021 mandible in medial view. **b**, ELGOL2016 021 in lateral view. **c**, ELGOL2016 021 in dorsal view. **d-h**, NMS G1992.47.10 preserving right dentary and premaxilla, with dentary in (d) occlusal, (f) lingual, and (h) buccal views, and premaxilla in (e) lingual and (g) buccal views. **i**, NHMUK PV R16331 frontal from Kirtlington in dorsal and ventral views. **j**, NHMUK PV R12680 left premaxilla from Kirtlington, in dorsal, lingual, and buccal views. **k**, NHMUK PV R12678 left dentary from Kirtlington, in posterior, lingual, and buccal views. **l**, NHMUK PV R12679 anterior tip of right maxilla from Kirtlington in buccal and lingual views.

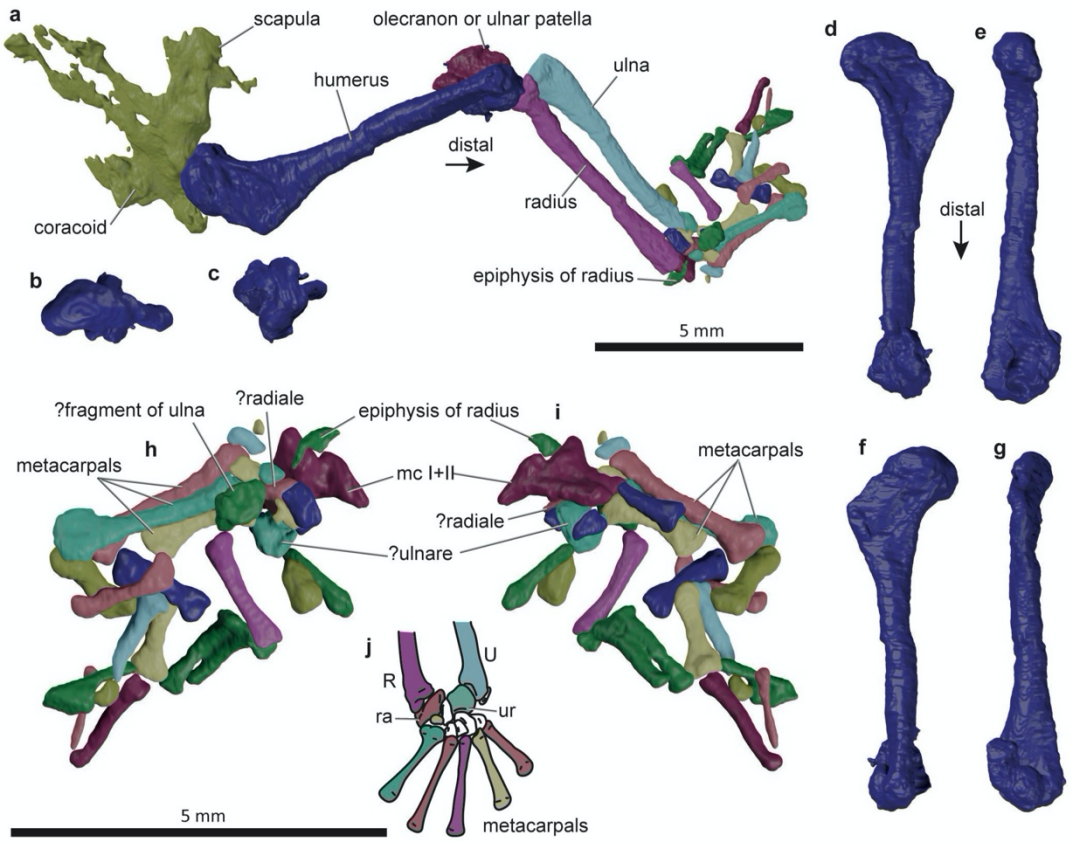

Extended Data Fig. 5. Forelimb

Left forelimb of *Bellairsia*. **a**, Whole preserved limb. **b-g**, Humerus in various views. **h-j**, Bones of the manus.

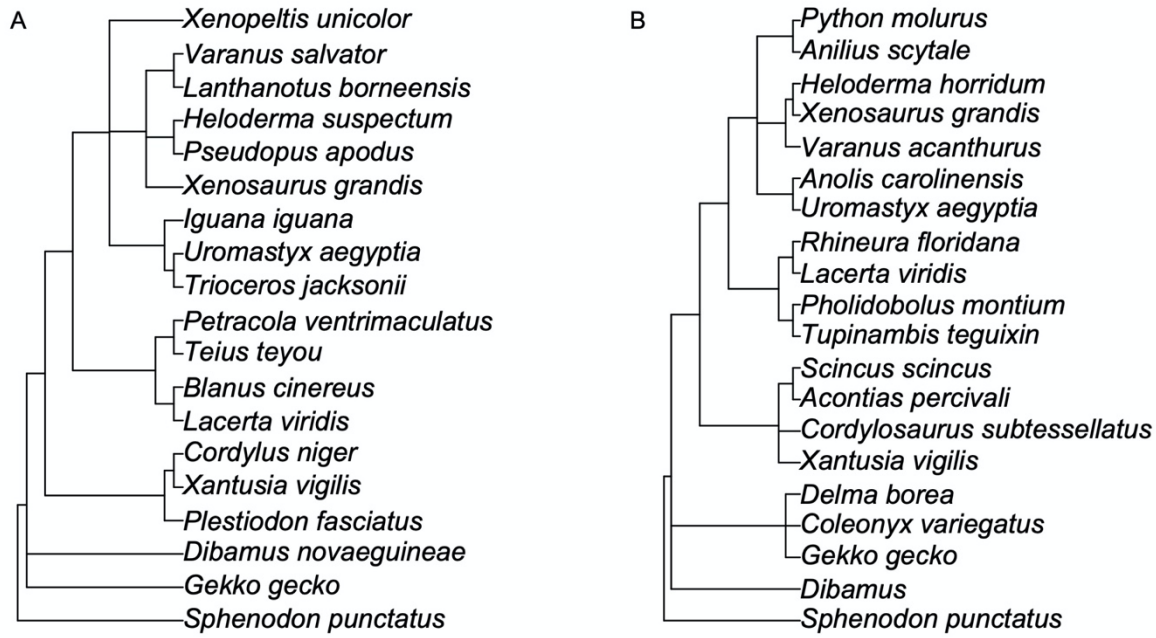

Extended Data Fig. 6. Molecular backbone constraint trees.
a, Constraint tree for Dataset 1 (dataset modified from ref. 24). **b**, Constraint tree for Dataset 2 (dataset modified from from ref. 28).

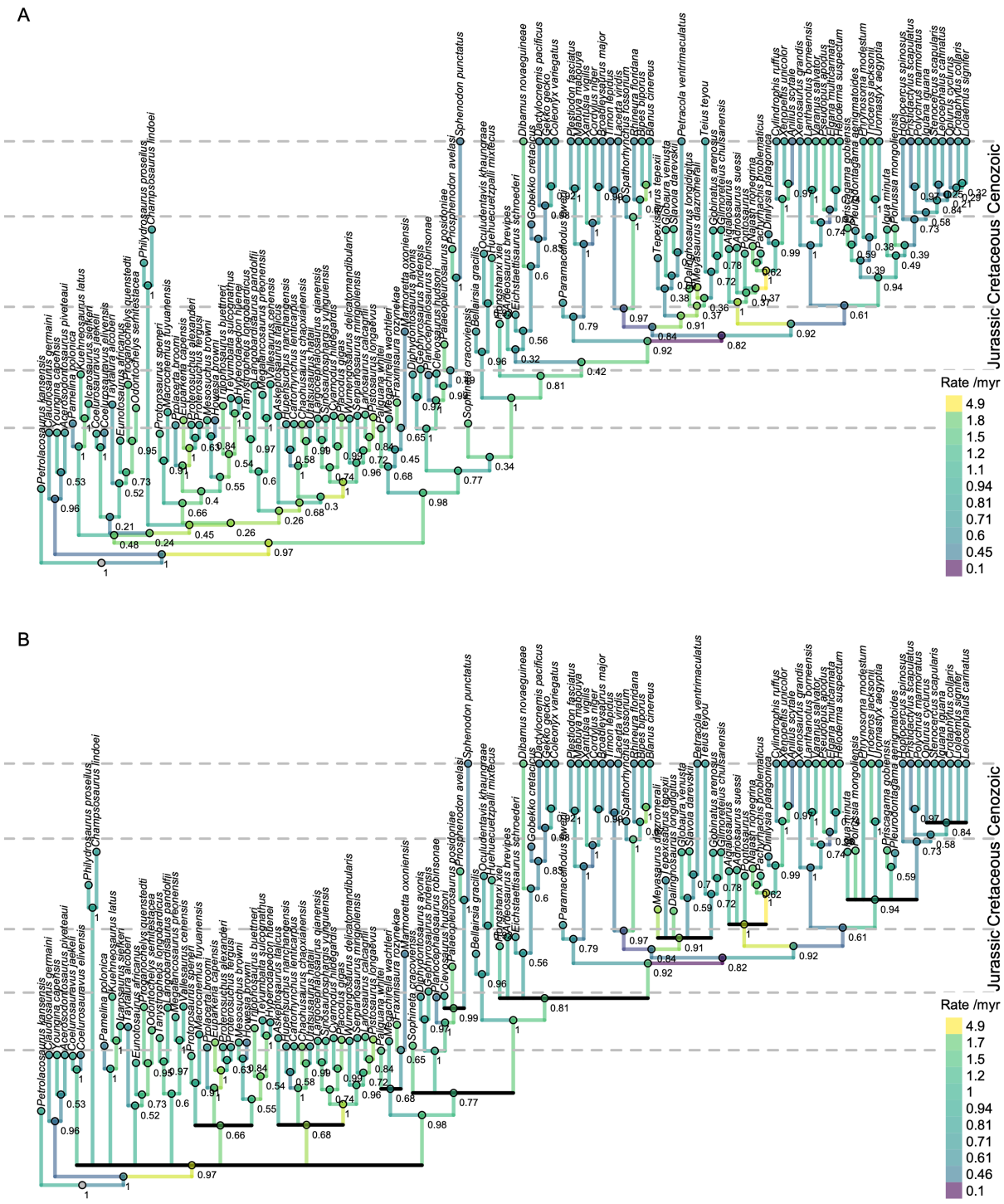

Extended Data Fig. 7. Bayesian analysis of Dataset 1 with taxa omissions

Majority rule consensus tree from Bayesian analysis of Dataset 1 (modified from ref. [24]) including molecular backbone constraint and omitting taxa with unstable phylogenetic positions that limit resolution of the consensus tree (*Scandensia ciervensis* and *Vellbergia bartholomaei*). **a**, Majority rule consensus including nodes with posterior probability <0.5; **b**, Majority rule consensus excluding nodes with posterior probability <0.5.

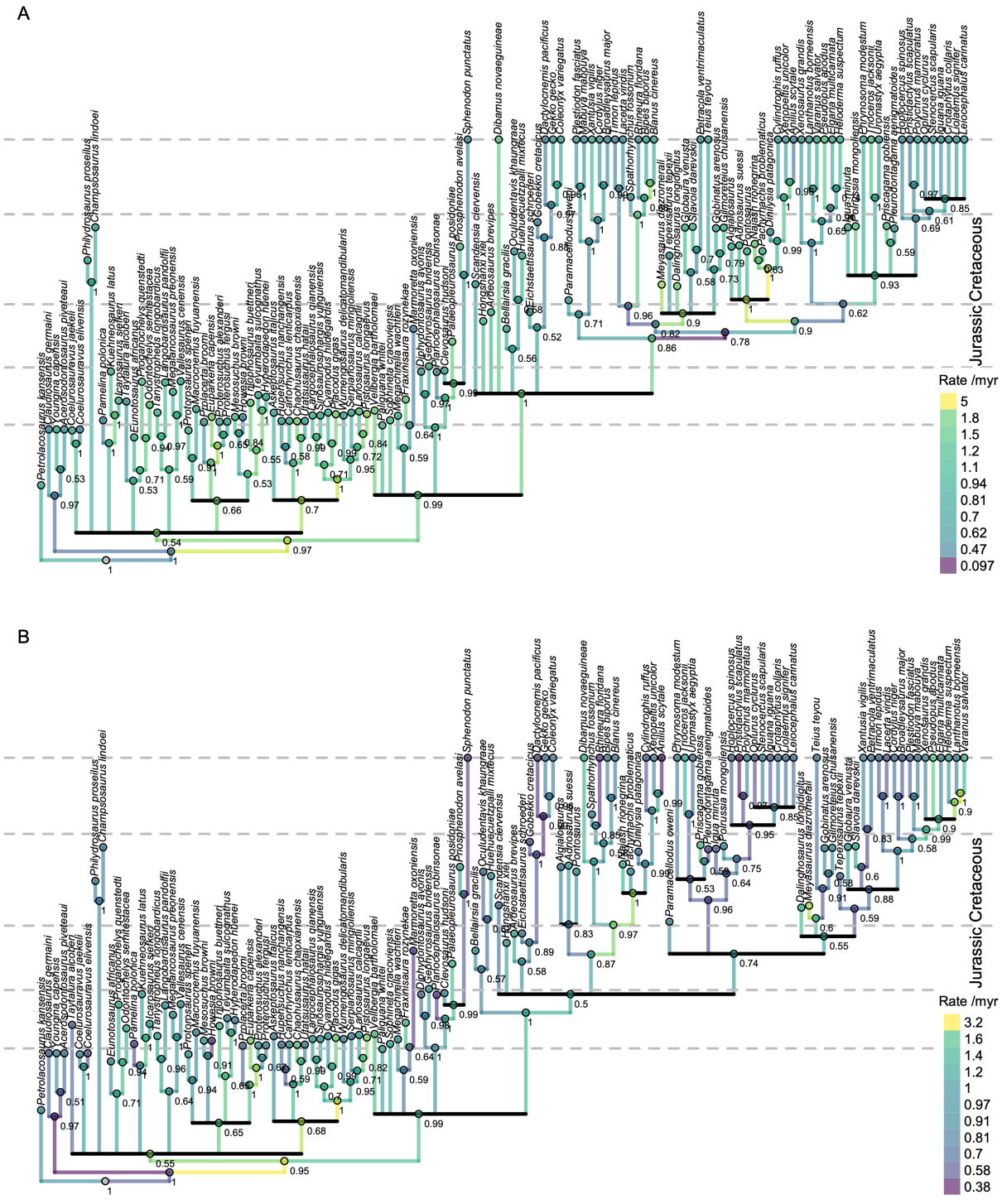

Extended Data Figure 8. Bayesian analysis of Dataset 1 without taxa omissions

Majority rule consensus tree from Bayesian analysis of Dataset 1 (modified from ref. [24]), not omitting any taxa. **a**, Tree from analysis including molecular backbone constraint; **b**, tree from analysis with minimal backbone constraint (constraining monophyly of extant squamates relative to *Sphenodon*).

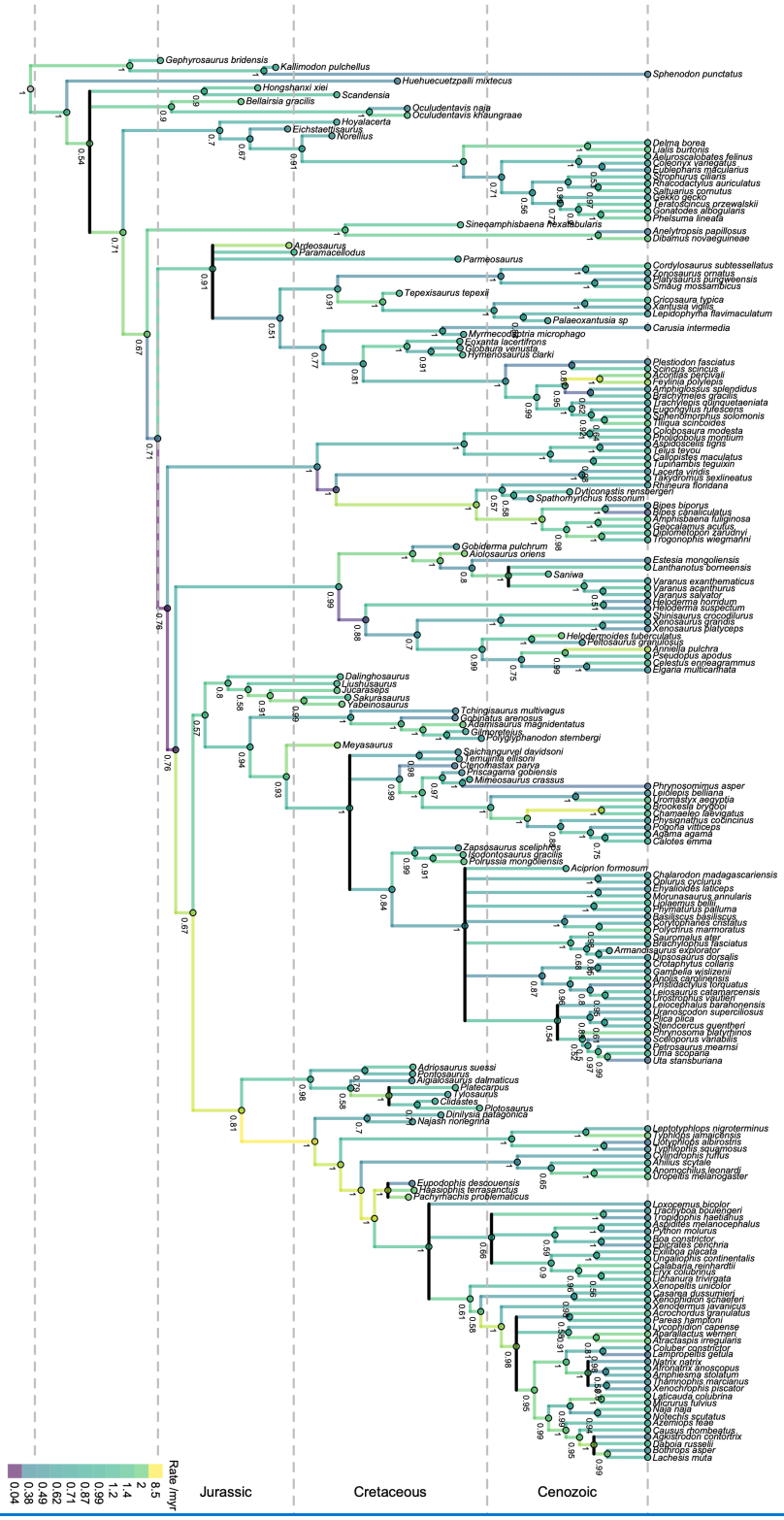

Extended Data Figure 9. Bayesian analysis of Dataset 2 with molecular constraint

Majority rule consensus tree from Bayesian analysis of Dataset 2 (modified from ref. [28]) including molecular backbone constraint.

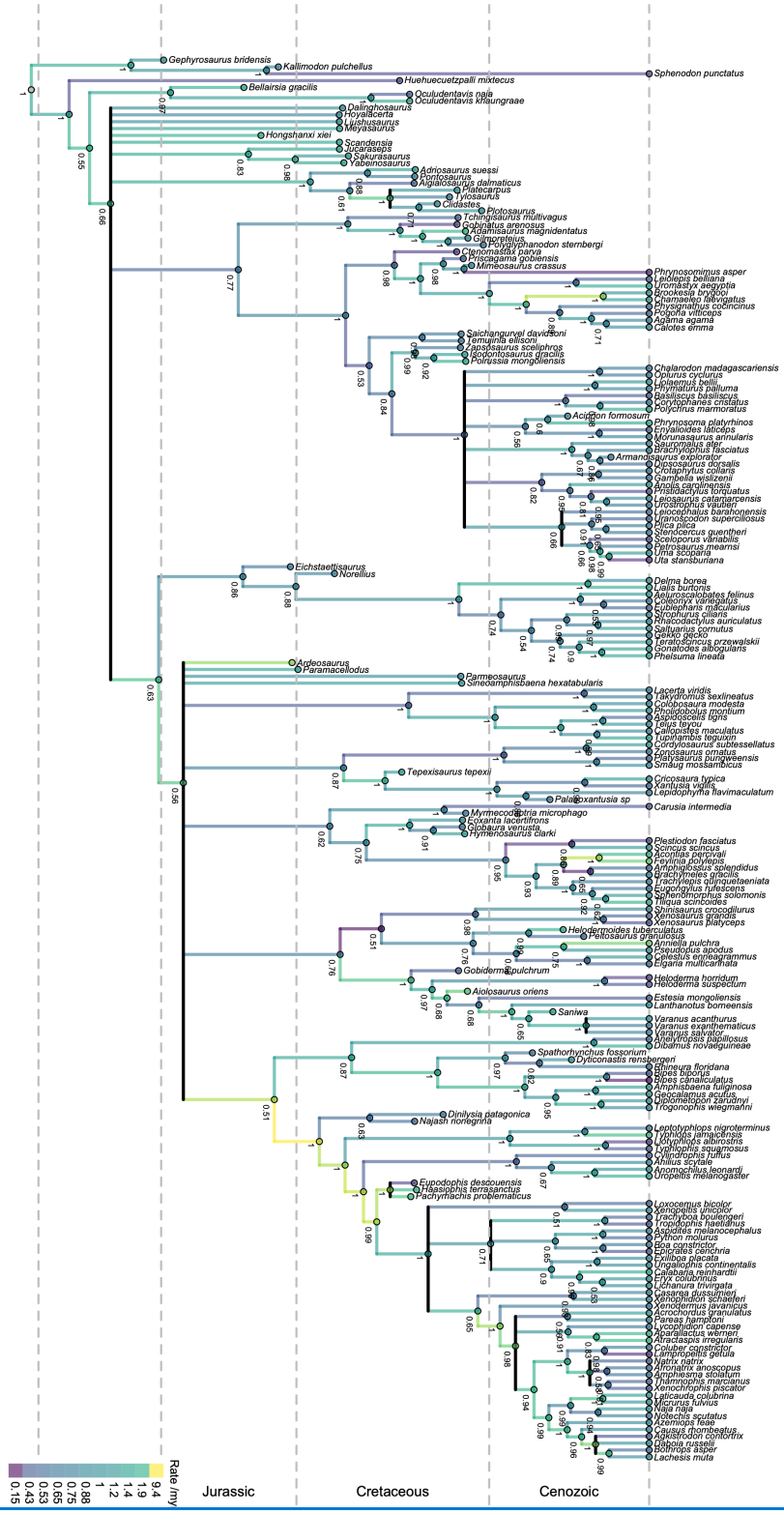

Extended Data Figure 10. Bayesian analysis of Dataset 2 without molecular constraint
Majority rule consensus tree from Bayesian analysis of Dataset 2 (modified from ref. [28]) without molecular backbone constraint.

Acknowledgements
M.T.'s work at UCL was financed by Mobility Plus programme (1608/MOB/V/2017/0) from the Ministry of Science and Higher Education, Poland. We thank the John Muir Trust and NatureScot for permission to carry out fieldwork on the Elgol Coast SSSI under permit. We thank Stig Walsh, Andrzej Wolniewicz and Richard Butler for support and assistance with fieldwork, and the Oxford University John Fell Fund and National Museums of Scotland for funding fieldwork. We thank Scott Moore-Faye for partial preparation of the specimen, and Luke Parry for assistance with running MrBayes on a computer cluster. Synchrotron tomography was carried out at the European Synchrotron Radiation Facility.

Author contributions
MT, RBJB and SEE planned the research. RBJB and EP collected new specimens. RBJB and VF scanned the specimens. MT segmented the CT data, wrote the description and drafted the manuscript with RBJB and SEE. MT and EP constructed the figures. MT, RBJB and SEE conducted the phylogenetic analysis. All authors provided feedback on the manuscript.

Declaration of interests
The authors declare no competing interests.

Extended Data and Supplementary Information is available for this paper.

Correspondence and requests for materials should be addressed to Roger Benson.

Supplementary Information
Systematic Palaeontology; extended osteological description; comments on phylogeny and results; supplementary references; list of synapomorphies of particular clades.

SI Guide

Supplementary Information.pdf

The file includes ‘Systematic Palaeontology’ section, extended osteological description, comments on the phylogenetic analysis and results, supplementary references, and a list of synapomorphies of particular clades.

Supplementary Information

Synchrotron tomography of a stem-lizard elucidates early squamate anatomy

Mateusz Tałanda, Vincent Fernandez, Elsa Panciroli, Susan E. Evans, Roger J. Benson

TABLE OF CONTENTS

Part 1. Systematic Palaeontology

Reptilia Laurenti, 1768

Lepidosauria Haeckel, 1866

Pan-Squamata Gauthier and de Queiroz, 2020

Bellairsia Evans, 1998

Bellairsia gracilis Evans, 1998

Holotype: partial left dentary, NHMUK PV R12678.

Referred specimens: NMS G.2022.1.1., a near-complete skeleton from the Bathonian Kilmaluag Formation of the Elgol SSSI, plus more fragmentary specimens referred by [18], including a dentary (NMS G.2019.34.1) and associated dentary and other elements (NMS G.1992.47.10). Additional remains are also known from the holotype locality, Kirtlington Old Cement Works, including a premaxilla (NHMUK PV R 12680), maxilla (NHMUK PV R12679), and frontals (NHMUK PV R16331). Tomographic scan data and 3D models for all these specimens are available at www.morphosource.org/projects/00000C672 .

Type locality: Kirtlington Old Cement Works Quarry, Oxfordshire, England. OS SP495200.

Type horizon: Kirtlington Mammal Bed, near base of Forest Marble (*aspidiodes* Zone, Layer 3P of [51]), late Bathonian (Middle Jurassic).

Original diagnosis [21]:

A small, gracile taxon characterised by long, parallel-sided dentaries, well-developed subdental ridge bearing splenial facet; 20-25 slender pleurodont teeth with tapering, lingually striated tips, and lingual tooth replacement; short, weak ventral muscle scar on dentary; maxilla with slender premaxillary process and small medial lappet; paired premaxillae each with 4-5 teeth, well-developed palatal shelf and narrow, tapering nasal process; frontals fused with weak cristae cranii (subolfactory ridges), without sculpture but grooved for overlying large head scales, no postfrontal/postorbital facets.

The characteristic features of the dentary (slender, parallel-sided, tooth morphology) and frontal (fusion, grooves, absence of postfrontal facets) are confirmed in the Skye material.

Emended diagnosis:

A small, gracile taxon characterised by long, parallel-sided dentaries, well-developed subdental ridge bearing splenial facet; 20-25 slender pleurodont teeth with tapering, lingually

striated tips, and lingual tooth replacement; short, weak ventral muscle scar on dentary; maxilla with slender premaxillary process and small medial lappet; paired premaxillae each with 4-5 teeth, well-developed palatal shelf and narrow, tapering nasal process; frontals fused with weak cristae cranii (subolfactory ridges), without sculpture but grooved for overlying large head scales, no postfrontal/postorbital facets. *Bellairsia gracilis* resembles crown-squamates and differs from rhynchocephalians in the complete enclosure of the vidian canal of the basisphenoid; the division of the metotic fissure into a separate dorsal vagus foramen and ventral recessus scala tympani; fully pleurodont dentition with continued tooth replacement; reduced palatal dentition; reduction of quadrate-pterygoid overlap to a small ventral lappet; fossa columellae in pterygoid forming synovial joint socket for epipterygoid; scapulocoracoid with scapular, scapulocoracoid, and primary coracoid emarginations. However, *Bellairsia* differs from crown squamates, except most gekkotans, in combining notochordal vertebral centra, and retaining intercentra throughout cervical and dorsal vertebral series. It further resembles gekkotans in lacking a parietal foramen and having a reduced postorbital bar, but differs from them in the pterygoid-vomer contact, fused parietals, shallow frontals without ventrally extended subolfactory flanges, open Meckelian fossa.

Elgol site (Kilmaluag Formation), Isle of Skye, Scotland

Scottish specimens of *Bellairsia gracilis* were collected from the Bathonian (Middle Jurassic) Kilmaluag Formation of the Elgol Coast Site of Special Scientific Interest (SSSI) on the west coast of the Straithaird Peninsula north of Elgol approximately 1 km south of Cladach a'Ghlinne [18,52]. NMS G.2022.1.1 was discovered by E. Panciroli in Spring 2016 and collected under field number ELGOL 2016.021.

Assignment of NMS G.2022.1.1. and other specimens from the same locality to *Bellairsia gracilis*

Bellairsia gracilis was erected by [21] based on isolated partial left dentary (NHMUK PV R12678) from Mammal Bed in Kirtlington Old Cement Works quarry (Oxfordshire, England) dated as Bathonian (Middle Jurassic). Other isolated bones, namely a premaxilla (NHMUK PV R 12680), maxilla (NHMUK PV R12679), frontals (NHMUK PV R16331), and several further dentaries and frontals from the same horizon were referred to this taxon based on their size, morphology (e.g. shared tooth morphology and articular facets) and high individual frequency in the assemblage suggesting that they belong to a single, abundant taxon. These elements have not previously been reported together in a single specimen that would confirm their association to a single taxon.

NMS G.2022.1.1. (field number: ELGOL 2016.021) represents most of the skeleton of a small lizard in articulation including posterior portions of both dentaries and maxillae, as well as a nearly complete frontal, and provides an excellent opportunity to test such hypotheses of association. The dentary of the new specimen shares a number of diagnostic

features with the holotype dentary of *Bellairsia gracilis* (NHMUK PV R12678): parallel-sided dorsal and ventral margins of the dentary, well developed subdental ridge with extensive splenial facet, indistinct ventral muscle scar, and chisel-like pleurodont teeth with tapering tips and lingual replacement. The presence of lingual striations on the tooth tips of NMS G.2022.1.1. could not be determined due to insufficient scan resolution of the scans. However, all other characters of the dentaries of NMS G.2022.1.1. link it to *Bellairsia gracilis*. Such attribution is additionally supported by relatively small size of the specimen, and its geographic and temporal proximity to Kirtlington Quarry.

The morphology of NMS G.2022.1.1. also confirms the accuracy of the original referral of isolated frontals from Kirtlington to *Bellairsia gracilis* by [21]. Frontals from Kirtlington share several features with NMS G.2022.1.1.: they are fused into a single element; they bear Y-shaped scars from overlying head scales but otherwise they have an unsculptured dorsal surface; they have the same structure of the frontoparietal suture; and they lack a facet for postfrontal or postorbitofrontal.

Unfortunately the premaxillae and anterior portions of the maxillae are missing in NMS G.2022.1.1., providing no overlap with the other elements from Kirtlington originally referred to *Bellairsia gracilis*. However, the tooth preserved in the premaxilla from Kirtlington (NHMUK PV R12680) matches those from the dentaries and maxillae of NMS G.2022.1.1. The two teeth preserved in the maxilla from Kirtlington (NHMUK PV R12679) have poorly preserved tips making any comparisons difficult.

NMS G1992.47.10 is a right dentary with associated premaxilla and other elements reported by [39] (fig. 4, as Scincomorpha indet.). This specimen was referred to *Bellairsia* by [18]. The dentary is 12.5 mm long and displays similar anatomy to that of the, less complete, holotype dentary (NHMUK PV R12678, Extended Data Fig. 4). The dentary is low relative to its length. The dorsal and ventral margins are subparallel to each other. The lateral surface bears a series of nine distinct foramina close to its anteroventral margin. Each foramen opens in a slightly different direction and the distances between each two foramina are very variable. Posteriorly the dentary bifurcates into dorsal and ventral processes of similar length and width. The bone is slightly bowed medially. The dentary tapers anteriorly due to an oblique upper margin and ends with a small symphysis. The symphysis is flat and anteroposteriorly longer than high. It is located just above the Meckelian groove. The groove opens ventromedially. The subdental shelf is well developed. The shelf bears a facet for the splenial in its posterior part. There are approximately 25 tooth positions. All preserved teeth are broken and incomplete. They have a pleurodont implantation and display replacement gaps and pits in the mid-lingual part of their bases. The teeth are subcircular in cross-section at least in the preserved part.

The premaxilla of NMS G1992.47.10 is also from the right side of the skull and was not fused to the counterpart. The bone is L-shaped in anterior view. The medial suture is slightly interdigitating at the base while being straight on the nasal process. The nasal process is relatively broad through its length although the distal part is not preserved. It is straight and forms an angle of about 60° to the main part of the bone. The process is anteroposteriorly

flattened. It has a foramen at its base, located anteroposteriorly. The palatal shelf is well developed. The premaxilla has a narrow facet for maxilla. The bone bears five tooth positions and three of these have incomplete, pleurodont teeth. The teeth have only their bases preserved but it is clear that the teeth were relatively slender. The assignment of this premaxilla to *Bellairsia* is questionable. NMS G.2022.1.1. is missing premaxillae while the premaxilla NHMUK PV R 12680 from Kirtlington is different in the following aspects from NMS G1992.47.10. NHMUK PV R 12680 is more triangular in anterior view, has a broader facet for the maxilla, a much more slender nasal process, and a roughly straight medial margin.

Part 2. Extended osteological description

The specimen preserves parts of the skull and the anterior portion of the postcranium in partial articulation, although most elements are dorsoventrally compressed. The tail is missing, having been lost during collection, and only the first few caudal vertebrae remain. Based on the preserved portion of skeleton we estimate the snout vent length as roughly 60-70 mm. The specimen appears to be adult, or close to adult size, based on the co-ossification of the scapula and coracoid, the fusion of the pelvic elements (with some trace of sutures) and of the astragalus and calcaneum in the ankle, and the ossification of the long-bone epiphyses.

Skull

The skull roof is displaced ventrolaterally relative to the basicranium, due to crushing, and most of the snout is missing. The preserved part of the skull roof (complete parietal and frontal, posterior part of nasal) is about 10 mm long. The orbits are relatively large and, consequently, the frontal at its narrowest point is just 2.2 mm wide. The temporal region is poorly preserved but clearly shows open upper and lower temporal fenestrae.

The preorbital part of the skull is damaged, having been lost to erosion prior to discovery of the specimen. As a result, the specimen lacks premaxillae, septomaxillae, and vomers. The nasals may be fused but the preservation is not good enough to be certain of this. The right side of the nasal plate is the more complete, although it lacks its anterior portion. The dorsal surface is flat and smooth. It expands moderately posteriorly where it meets the frontal along a sinuous posterior margin. The facet for the frontal is visible posteriorly on the ventral surface of the bone. It has a subtriangular outline with its deepest point near the medial margin of the bone. The posterolateral margin of the nasal is marked by a slight concavity that bears a shallow facet for the prefrontal, but the nasal lacks a posterolateral process. A facet for the maxilla is not visible on the nasal, as preserved.

The left side of the frontal is damaged anteriorly, but the right side is complete. The frontals are firmly co-ossified on the midline with no suture evident. However, the anterior part of the bone bears a narrow sagittal groove on the dorsal surface. This groove could be a remnant of the suture between frontals or may simply mark the position of the low ridge on the ventral surface that separates parts of the olfactory chamber. The frontal has no surface ornamentation, but the posterior part of its dorsal surface bears a shallow Y-shaped groove that most likely marks the position of large head scales. Anteriorly, the frontal bears a well-developed shelf that underlapped the posterior parts of the nasals. The shelf expands anteriorly close to the midline and is embayed by a shallow V-shaped notch where the nasals met. The outline of the anterior margin of the frontal, as visible when the nasals are in articulation, has a sinuous outline. A small anterior process is flanked by small notches, lateral to which on the preserved right side is a shallow embayment. An anterolateral process is not developed. The lateral edge of the frontal forms the medial and posteromedial margins of the orbit and is concave through the whole of its length. Anterior to the orbit, the lateral edge of the frontal bears a long facet for the prefrontal, occupying more than one third of the frontal

length. This facet is oriented ventrolaterally, and so is visible in ventral, but not dorsal, view. The posterior margin of the frontal is almost straight across most of its width but is developed laterally into a pair of well-developed posterolateral processes. These bear facets for the parietal on their ventral surface, whereas the central section of the frontal bears a narrow shelf that underlaps the parietal ventrally, suggesting that the frontal and parietal fitted quite firmly together. However, there is no trace of a posterolateral facet for the postfrontal. The ventrolateral margins of the frontal display shallow subolfactory ridges (cristae cranii) and there is a distinct ventral sagittal ridge in the anterior half of the bone.

The parietal is preserved in left and right parts, with the latter strongly deformed. However, a cross-section of the bone shows that it is broken rather than sutured in the midline, and that the parietal was therefore unpaired in-life (i.e. the midline suture of the parietals was fully closed). There is no trace of a parietal foramen. The main, central part of the dorsal surface of the parietal is convex, flattening out laterally. The anterior margin of the parietal bears facets for the frontal. The lateral margin is concave and forms the medial margin of the upper temporal fenestra. The attachment surfaces for the adductor muscles are present on the lateral margins of the parietal. These margins are shallow, oriented ventrolaterally, and are bounded by distinct ridges along the margins of the ventral surface. These ridges continue onto the ventral surface of the posterolaterally projecting supratemporal processes. There is no epipterygoid process anteriorly. Along the posterior margin of the bone, the nuchal surface is shallow and extends into a median postparietal projection.

Only the posterior parts of the maxillae are preserved, indicating a minimum of eleven tooth positions, although the original number was likely much greater given a dentary count of around 25. The facial process is damaged and its original shape is therefore unknown. The preserved posterior part is mediolaterally thin, and thus easily damaged. One large nutrient foramen (anterior opening of the superior alveolar canal) opens at the base of the preserved portion of the facial process. The dentition is pleurodont. The tooth bases rest on a well-developed subdental shelf, and they are supported by a relatively deep labial wall. What may be part of the lingual wall (or of a maxillary shelf) is visible on the right maxilla. The posterior process of the maxilla tapers distally. Its dorsal surface bears two narrow, anteroposteriorly elongate facets: a dorsal facet for the jugal and a medial facet for the ectopterygoid.

The prefrontals are damaged and incomplete due to erosion and compaction. The dorsal part is expanded to meet the frontal dorsally and posterodorsally, and the nasal anterodorsally. Its margin is straight and did not contribute to the skull roof. On the right bone, a large nutrient foramen is visible on the dorsolateral surface, just anterior to the orbital margin. The prefrontals form the entire anterior margin of the orbit, with the orbital margin marked by a well-developed medial orbitonasal flange. The posteroventral part of each bone tapers distally but nevertheless contacts with the jugal, lacrimal, maxilla, and ectopterygoid. The prefrontals are also in contact with the maxilla anteroventrally, but the anterior portion is damaged, and its exact shape is difficult to reconstruct. Nevertheless, the prefrontals clearly formed a significant part of the lateral wall of the snout.

The lacrimals are present on both sides of the skull but they are slightly displaced anteriorly on the right side and posteriorly on the left. Only the right bone is fairly complete, although its dorsal margin is damaged and difficult to reconstruct. The lacrimal slotted between the maxilla and prefrontal. Its lateral surface displays a facet for the maxilla that expands anterodorsally and is pierced by a small foramen. The medial side of the lacrimal is flat, except for a posteroventral projection that tapers distally, and was originally located along the dorsal margin of the maxilla. The projection is slightly curved, framing a lacrimal duct positioned between the lacrimal and prefrontal.

The postfrontals are very small compared to other skull bones. They are dorsoventrally flattened and quadriradiate. The two largest processes were probably positioned anteromedially and posteromedially, and the two smaller ones were directed laterally. The two pairs of processes lie in slightly different planes. What we interpret as the medial surface of the bone is smooth, with no obvious facet for the frontal or parietal. This suggests the contact between the postfrontal and skull roof was ligamentous, an interpretation consistent with the lack of a postfrontal facet on the frontal. There is a shallow facet on the lateral margin that may be for a postorbital, but no postorbital was identified on either side of the specimen. A group of bone fragments next to the posterior end of the right jugal might represent the remains of the postorbital, but this identification is tentative.

The left jugal seems to be nearly complete, whereas the right jugal lacks its anterior and posterior ends. The jugal is a large and robust bone compared to the preserved portion of the maxilla. It is moderately bowed at a wide angle, reflecting the curvature of the ventral margin of the orbit. The anterior portion of the jugal is robust and subtriangular in cross-section, forming a distinct medial ridge. Its ventrolateral surface bears a distinct elongated facet for the maxilla that expands anteriorly. In contrast, the posterior lamina of the jugal is delicate and mediolaterally flattened. The transition between the anterior (orbital) and posterior lamina is abrupt on the medial side of the bone, with the medial ridge slightly overhanging the anterior margin of the posterior lamina. The jugal bears a very short posterior process. The postorbital process is dorsomedially flattened and tapers distally. This process is very short and of comparable length to the posterior process. If it is not a preservational artifact, the short postorbital process could mean that the jugal was not in bony contact with the postorbital or postfrontal. The lateral surface of the jugal is pierced by nutrient foramina that enter the bone at various angles. These are poorly preserved in the anterior part of the bone.

We could not identify any element that could be interpreted unambiguously as squamosal. A flattened, rod-like, element lying near the squamosal notch of the quadrate, and protruding a short distance anterior to it, is a possible candidate.

Both quadrates are poorly preserved. They were compressed and displaced by the mandibles during compaction. The following description is based on the better-preserved left quadrate. The dorsal part of the bone is damaged. The remainder expands ventrally into hourglass-shaped condyles for the mandible. The anterior surface of the bone displays a small foramen that lies just above the condyles, and a pterygoid lappet medially. The lappet is well developed and is directed anteriorly, but it is restricted to the ventral margin of the bone and

differs strongly from the large overlapping pterygoid wing found in stem-lepidosaurs like *Marmoretta* [23] and in rhynchocephalians like *Sphenodon* and *Gephyrosaurus*[53]. The quadrate conch is well-developed but shallow. The squamosal notch is deep.

Parts of the palate are preserved. However, as with the rest of the skull, the anterior parts are missing, and the vomers have not been identified. The palatines are delicate and were crushed during compaction. The left is better preserved than the right and the following description is based solely on it. The palatines were separated in the midline by the pterygoids. The vomerine (anteromedial) process is complete and unbroken but is small, triangular, and indistinct. The maxillary (lateral) process is anterolaterally directed. It is more robust and reaches further anteriorly than the vomerine process. Its ventral aspect bears a relatively large foramen probably for the maxillary division of the trigeminal nerve. There is no trace of choanal groove. The palatine plate tapers posteriorly. Its medial margin met the pterygoid whereas the lateral margin is concave and contributed to the border of the suborbital fenestra. There is no trace of palatine teeth.

Both pterygoids are preserved but they are broken and the right one is heavily damaged. The pterygoid is a triradiate bone with a well-developed lateral flange, and anterior and posterior processes. A small oval group of denticles is present in the centre of the ventral surface. The lateral flange and anterior process are dorsoventrally flat whereas the posterior process is robust and subcircular at its base. The anterior process is complete in the left pterygoid although broken at its base. It is relatively narrow and its base is no wider than the posterior process. It tapers rostrally, extending to the level of the anterior margin of the palatine excluding it from the interpterygoid vacuity. The lateral margin of the anterior process of the pterygoid bears a long, oblique palatine facet. The medial margin of the anterior process of the pterygoid is thickened but it was not in contact with the contralateral pterygoid. The tip is dorsoventrally thickened and bears a figure-of-eight-shaped facet for vomer. The lateral flange of the pterygoid is subtriangular in dorsal view and forms the wide posterior margin of the suborbital fenestra. Its lateral tip forms a distinct process, directed anteriorly at a right angle to the rest of its anterior margin, and bearing a facet for the ectopterygoid. The distally tapering posterior process of the pterygoid is the most robust part of the bone. Its ventromedial surface bears a distinct fossa for the basipterygoid process of the braincase. Dorsally there is an oval dorsal pit (fossa columellae) for the epipterygoid.

Both ectopterygoids are preserved. They are nearly complete and are undeformed. Each bone is slightly curved rather than L-shaped and bears a small lateral flange along its central part. It is gently bowed along its medial side, where it frames the suborbital fenestra, and straight on its lateral side. The ectopterygoid tapers anteriorly to a pointed tip where it bears a ventral facet for the maxilla. The bone was also in contact with the jugal and probably the maxillary process of the palatine. Posteriorly, each ectopterygoid bears a pocket facet for the pterygoid.

The braincase is dorsoventrally crushed. A fragment with a spherical cavity on the left side of the braincase might represent the supraoccipital, the cavity representing the dorsal component of the cavum capsularis. A second element preserved in this area may be the left prootic. However, individual structures are difficult to interpret due to poor preservation. The

basisphenoid is flattened and broken in several places. The basipterygoid processes are long and slender, with expanded distal ends. The processes are pierced at their base by the vidian canal, which is thus restricted to the basisphenoid. The foramen for cranial nerve VI (abducens) appears above the anterior opening of the vidian canal. The bases of the trabeculae cranii are visible between the basipterygoid processes, but we could not detect the parasphenoid rostrum. The crista sellaris is low and vertically oriented. On the basioccipital, the basal tubera are well developed. The lateral opening of the recessus scalae tympani is visible next to the right basal tuber. It forms an occipital recess, bordered posteroventrally by a crista tuberalis. The basioccipital is firmly fused with the exoccipital, with no visible suture between the two bones. The exoccipital is pierced by a pair of foramina for the hypoglossal nerve. The oto-occipitals are compacted on both sides of the basioccipital, but it is not possible to determine whether they were fused to the exoccipitals. A crushed posterolateral portion of the cavum capsularis is visible on the right side of the braincase. The left paroccipital process is displaced ventrally and rotated anteromedially. Its distal tip remains in contact with the quadrate.

Mandible

Only the posterior parts of each dentary are preserved in NMS G.2022.1.1., but other specimens preserve different portions (NHMUK PV R12678; NMS G.2019.34.1), and a near-complete dentary are present in NMS G1992.47.10, missing tooth apices (Extended Data Fig. 4). The more complete left dentary of NMS G.2022.1.1. has six tooth positions remaining, although many more would have been present anterior to this prior to breakage. The teeth are supported by a well-developed subdental shelf that bears an anteroposteriorly-oriented facet for the splenial. The Meckelian fossa occupies the rest of the bone below the shelf. The preserved portion of the dentary has subparallel dorsal and ventral margins. Posteriorly it forks into two distinct processes of similar length. The dorsal process is dorsoventrally wider than the ventral process. The splenials are very damaged. Their anterior extent remains unknown, but they extend posteriorly to the level of the coronoid process. The anterior mylohyoid foramen perforates the anterior part of the splenial as preserved, and there is also a smaller foramen located posteroventrally.

The right coronoid is well preserved. Its dorsal (coronoid) process is well developed, but a labial process is absent. The anteromedial process of the coronoid is long, reaching the level of the last tooth position of the dentary. It wraps over the dorsal margin of the dentary, extending only slightly onto the labial surface. Lingually, the anteromedial process bears a distinct medial facet for the splenial. The posteromedial process of the coronoid is damaged. It is of similar length to the dorsal process and extends ventrally over the medial surface of the surangular to contact the prearticular. The posterior process of the coronoid is very small and sits dorsally on the surangular.

The angular forms the ventral part of the mandible posteriorly over much of the preserved length and is well exposed on the lateral side of the mandible, where it forms about one fifth of the depth of the bone at the level of the coronoid process. The anterodorsal part of the

angular bears an anterior facet for the dentary which it contacts beneath the prearticular and surangular. It has a smaller exposure medially than laterally and is covered anteriorly by the splenial. The surangular forms the dorsal part of the mandible over much of its preserved length. It bears a large lateral facet for the dentary on its anterodorsal surface, a dorsal facet for the coronoid, and a long ventral facet for the angular. The anterior half of the angular facet faces medially, and the posterior part faces laterally. The anterior surangular foramen is large and lies ventral to the coronoid, just anterior to the peak of the coronoid process. The posterior surangular foramen could not be detected, most likely due to poor preservation of the posterior part of the bone. A facet for the prearticular is visible on the medial surface of the surangular, dorsal to the angular. The prearticular forms an elongated anterior process that projects between the surangular and angular. It bears an elongated anterior facet for the splenial and a ventral facet for the angular. The anterior part of the prearticular is covered by the splenial, thus obscuring any possible contact with the anteromedial process of the coronoid. The prearticular is fused with the articular. The latter is damaged, but has a well-developed retroarticular process with a sharp lateral crest.

Two long ceratobranchial elements are present beneath the skull bones.

Dentition

The tooth implantation is pleurodont in both the dentaries and maxillae. The teeth are unworn. Those of the maxilla are very similar to those of the dentary. They have a chisel-like appearance. The base is subcircular in cross-section, but the crown is labiolingually flattened. The tip is not sharp, but it is directed slightly lingually. The crown bears apicobasally-oriented anterior and posterior grooves on its lingual surface. These grooves converge towards the crown apex but fail to meet. The tooth rows show lingual replacement pits and gaps for unimplanted teeth. On the right dentary, an erupting tooth appears to be eroding the posterolingual surface of the first preserved tooth and the anterolingual margin of the tooth following it. On the maxilla, the replacement pits are more typically placed in the mid-lingual part of the erupted crown bases.

Axial skeleton

The axial column is preserved in partial articulation. The articulated series is sinuous due to post-mortem anterior displacement of the pelvis and posterior dorsal vertebrae, which has introduced a prominent kink to the vertebral series. The vertebrae remain in anatomical order although they are crushed. *Bellairsia* has 24 presacral vertebrae in total. They are deeply amphicoelous and notochordal. Intercentra persist along the whole presacral vertebral column. They are not fused with the vertebrae and are positioned intervertebrally.

The neck is poorly preserved. The cervical elements are compacted, slightly displaced and surrounded by bony fragments. The neural arches of the cervical vertebra are usually detached from their centra and are poorly preserved. The centra bear a mid-ventral sagittal ridge. Both

halves of the atlantal neural arch are preserved although they are detached from the axial column. The ventral part of each atlantal arch is markedly expanded and circular in cross-section. The dorsal part is flattened. The left arch is more complete and preserves a postzygapophysis. A subtriangular element lies anterolateral to the atlantal neural arches. It is most likely the first (atlantal) intercentrum. The bone is anteroposteriorly short relative to its width. The main part is crescent-shaped and shows a contact area for the axis. The hypapophysis is directed ventrally. The distal portion is thicker anteroposteriorly than transversely. The tip of the hypapophysis is blunt and unexpanded.

The axis is poorly preserved and its neural arch is damaged. The posterior part of the centrum shows that it is clearly amphicoelous. The first and second intercentra were not detected, but whether they were absent in life or displaced post-mortem is unknown.

The pre- and postzygapophyses of the postaxial vertebra (cervical 3) are well-developed although their original inclination is difficult to reconstruct due to compaction. The cervical neural spines are well-developed. They are directed posterodorsally and have a rounded outline in lateral view. The third intercentrum resembles the following cervical intercentra. It is kidney-shaped, bearing a small pointed hypapophysis. Due to poor preservation, it is uncertain which cervical vertebra bore the first pair of ribs, but they were certainly present on the fourth and more posterior cervicals, although the adjacent ribs are displaced anteriorly. The anterior cervical ribs have expanded and flattened distal ends.

All dorsal vertebrae bear ribs. The anterior dorsal ribs are curved and slender, and are much longer than the cervical ribs. However, the ribs decrease in length in the posterior trunk and become straighter. The sacral vertebrae are crushed against the pelvis. They are shorter than the posterior dorsals. Two anterior caudal vertebrae are preserved. They are crushed by compaction and are surrounded by numerous bone fragments. Their centra resemble those of the presacral vertebrae, but the neural arches are obliterated.

Pectoral girdle and forelimb

The interclavicle is not preserved but is inferred to have been present because the clavicles bear a ventromedial facet for it. Bony fragments posterior to the skull might be remnants of the interclavicle as the other bones of pectoral girdle are displaced anteriorly. The incomplete clavicles are straight and taper to a sharp tip distally. The scapula and coracoid are fused to each other on both sides of the specimen, and there is a shallow scapulocoracoid embayment. The scapula has a relatively short shaft and is moderately expanded dorsally. It is deeply embayed by a scapula emargination. The coracoid is well-developed and is pierced by a supracoracoid foramen. The bone contributes to the glenoid cavity. Anteriorly the coracoid is deeply embayed by a primary coracoid emargination.

Both humeri are preserved although the left one is in better condition. It is 9 mm in length. Its proximal and distal ends are expanded (in the pre- to postaxial plane) and rotated by about 90° to each other. The epiphyses are evident as separate ossification centres, but are correctly

articulated with the diaphysis, suggesting firm attachment. The degree of fusion could not be evaluated in detail due to resolution. The deltopectoral crest is well developed and thickened distally. It has a subtriangular outline and occupies more than a quarter of the humeral length. The distal condyles are well developed but the presence or absence of an ectepicondylar foramen is uncertain. A large element that lies adjacent to the distal part of the humerus might be an ulnar patella or a detached olecranon process. In either case, it would be very large. The radius and ulna are of similar length to one another (6 mm) and both are relatively slender, although the ulna is expanded and slightly bowed proximally.

Both hands are preserved, but the bones are disarticulated and difficult to identify. There is a total of nine disarticulated elements at the proximal end of the left hand, with one further small element located distally among the phalanges. The latter could represent a displaced carpal or a poorly preserved phalanx or ungual. Another (more proximal) element probably represents part of the broken distal head of ulna. Under that interpretation, there were at least eight carpal elements (unless some are enlarged sesamoids), suggesting a relatively primitive arrangement. The two largest of the carpal elements probably represent the radiale and ulnare (Extended Data Fig. 5). Of the remaining carpal-like elements, the largest is ovoid and may be distal carpal 4. We cannot attribute the others with certainty due to their disarticulation. Amongst extant lizards, the carpus typically includes nine elements: two proximal carpals (radiale, ulnare); a centrale (usually homologized with the lateral centrale of *Sphenodon*); a distal row of five carpals; and a pisiform sesamoid adjacent to the ulnare[54]. In some lizards (e.g. *Gerrhosaurus nigrolineatus*[55]), there is an additional small element, usually homologized with the intermedium of *Sphenodon*, between the radiale and ulnare in the proximal row. It is possible that *Bellairsia* also had this element if all 10 elements were carpals. Within the manus itself, there is no trace of either specialization or reduction in the metacarpals (MC) and phalanges which show a typical lizard morphology. Judging from the number of the metapodials and phalanges, the hand probably had a typical phalangeal formula (similar to that of the foot, 2-3-4-5-4). The metacarpal shaft is subcircular in cross-section, with expanded proximal and distal ends. The lengths of MC I-V from the left hand are as follows: 1.1 mm, 1.4 mm, 2.6 mm, 2.5 mm, 1,45 mm. A rough estimate of digit 4th length is 6.3 mm. The whole hand may be as long as 9.5 mm.

Pelvis and hind limb

The right pelvis is preserved and is nearly complete. The ilium, pubis, and ischium are fused together, although some of the suture lines between the bones are visible. The iliac blade is oriented posterodorsally and bears a very indistinct blunt anterior tubercle. The blade expands dorsoventrally in the mid-shaft and tapers distally. The pubis is crushed especially in the symphyseal area. The obturator (pubic) foramen lies just below the acetabulum. Further distally, there is a pubic tubercle with a subtriangular outline and a blunt, thickened end. The two free margins of the tubercle form a right angle. The tubercle is broken and directed posteriorly so prior to compaction it probably protruded ventrally. More distally the whole pubis is directed medially and decreases slightly in its width. The distal part of the ischium

has a subrectangular outline. The posterior margin forms a right angle with the ventral symphyseal margin, and the ischial tubercle forms a similar angle. The ischium lacks an indentation for the hypoischium.

The hind limb is much longer than the forelimb (approximately 32.2 mm compared to 24.5 mm). The pes is the longest segment although its exact length is difficult to determine due to poor preservation of the distalmost elements. The preserved pedal elements have maximum length of 14.5 mm in total. The complete foot was probably 15-15.5 mm long. The femur is gently curved and has a well-developed internal trochanter located close to the femoral head. It is 9.7 mm long, similar in length to the humerus (humerus/femur proportion 0.928). Both femoral epiphyses are present but are slightly dislocated suggesting that the sutures were not fully closed. The distal head is composed of two semicircular, ventrally-oriented condyles that are separated by the intercondylar groove.

The tibia is poorly preserved. The proximal head is damaged and the whole bone is crushed anteroposteriorly. The estimated length was ~7 mm. The distal end is slightly concave. This concavity was probably reduced in depth by compaction and suggests the presence of a notch on the distal epiphysis. The fibula is 7.1 mm long, slender and rod-like. Its mid-shaft diameter is almost one-third that of the tibia. The distal epiphysis of the fibula is detached, suggesting a lack of fusion.

The astragalus and calcaneum are fused. The large distal tarsal IV has a trapezoidal outline in dorsal view. It bears a distinct articular surface for the adjacent metatarsal. Distal tarsal III is much smaller. It is constricted mediolaterally and has a subquadrangular outline in lateral view. An element identified as a probable distal tarsal II is dislocated slightly posteriorly. It is the smallest distal tarsal and has a less regular shape. The metatarsals and phalanges are well ossified and have distinct joint surfaces. Metatarsals (Mt) I-IV are elongated and slender, with expanded proximal and distal ends. Of the four, metatarsal I is the shortest (2.6 mm), Mt II intermediate (3.9 mm), while Mt III and Mt IV are the longest (4.6 mm). Mt IV has the widest proximal and distal ends and is generally more robust than Mt III, despite having the same length. As usual, Mt V is hooked. It is only 2 mm long and is robust compared to other pedal elements. The distal head is rotated 90° relative to the proximal one. However, there is no trace of inflection. The lateral margin of the Mt V is straight. The outer process has a rounded outline in ventral view. The distal part of Mt V is about three times deeper dorsoventrally than the mid-shaft, due to the well-developed ventrally projecting lateral plantar tubercle. This tubercle is flattened at its pinnacle, which marks the attachment of the femoral head of the gastrocnemius muscle. Further distally, the tubercle becomes shallower and its surface grades into the distal articular surface without any clear boundary between the two structures. The medial plantar tubercle is a distinct mediodistally directed structure close to the proximal articular surface of MT V. It is much smaller than the lateral plantar tubercle. The phalangeal formula of the pes is 2-3-4-5-4. The unguals are curved, proximally deep and very narrow bilaterally. A sesamoid is preserved dorsal to the distal head of the first phalanx of the digit I.

Part 3. Comments on the phylogenetic analysis and results

Results of the main analysis found some support for a relationship between *Oculudentavis*, *Huehuecuetzpalli* and *Bellairsia* on the stem of Squamata (Extended Data Figs 7–8; Dataset 1, modified from refs [14,23,24], both when constrained to a molecular backbone and unconstrained, and when including or excluding taxa with unstable phylogenetic positions: *Scandensia* and *Vellbergia*). In the main analysis, this topology is supported by seven character states (see below) including the reduction and anterior positioning (relative to the parietal) of the postfrontal and likely absence of a parietal foramen, but many of the other supposedly shared traits are unknown in one or more of the three taxa. *Oculudentavis* and *Bellairsia* share some similarities like vaulted parietals, fused frontals that clasp the anterolateral margins of the parietal (as also in *Hongshanxi*), a short post-coronoid mandible, and ectopterygoid aligned anteroposteriorly. However, these are either absent or unknown for *Huehuecuetzpalli*, and there are also clear differences between *Bellairsia* and *Oculudentavis* including, in the latter, the nasal crest, the shape of the naso-frontal suture, the ring-like lacrimal, the palatal vacuities, the weaker coronoid process, and the long extremely slender dentary. Furthermore, although our analysis of Dataset 2 (modified from refs [11,28]) confirms that these taxa are stem squamates and returns a clade of *Bellairsia+Oculudentavis*, it finds *Huehuecuetzpalli* in a more rootward position (Extended Data Figs 9–10).

The Mid-late Jurassic (late Callovian-early Oxfordian) Chinese species *Hongshanxi xiei*[30] is one of the most complete early squamate fossils. It resembles *Bellairsia* in the lack of sculpture, median frontal, possible partial fusion of the nasals, deep jugal, and short broad median parietal without a parietal foramen, but differs in the large postorbital, extensive osteodermal cover over the temporal region, procoelous vertebral centra, and reduction of distal tarsal number to two. The original phylogenetic analysis[30], using the matrix of Gauthier et al.[11], found alternative positions for *Hongshanxi*, depending on whether the analysis was constrained to the molecular phylogeny, or unconstrained. The unconstrained analysis of ref. [30] placed *Hongshanxi* in an unresolved position on the stem of non-iguanian squamates; the constrained analysis placed it as a stem-squamate, sister taxon to the early Cretaceous *Scandensia* (see below). All our analyses of Dataset 1 place *Hongshanxi* in a polytomy at the base of the squamate crown group when collapsing nodes with posterior probability less than 0.5, or as a stem squamate crownward to *Bellairsia+Oculudentavis+Huehuecuetzpalli* when displaying these weakly-supported nodes (Extended Data Figs 7–8). Analyses of our Dataset 2 place *Hongshanxi* as the sister taxon of *Scandensia*, forming a stem squamate clade that is crownward to *Bellairsia+Oculudentavis* (when using a molecular backbone constraint for relationships within Squamata; Extended Data Fig. 9), or in a polytomy at the base of the squamate crown (not using a molecular backbone constraint for relationships within Squamata; Extended Data Fig. 10).

Another taxon placed on the squamate stem in the broader analyses is the Early Cretaceous (Barremian) *Scandensia ciervensis*[41,56]. Like *Bellairsia*, *Oculudentavis* and *Huehuecuetzpalli*, *Scandensia* has amphicoelous vertebrae, but it differs in having body osteoderms[56], an unusual rhomboid interclavicle[41], and exceptionally elongated penultimate phalanges[41, 56]. Unfortunately the skull of the holotype specimen is crushed and almost uninformative,

making comparison difficult. Our analyses of Dataset 1 return an uncertain position for *Scandensia* as a basal crown squamate or crownward stem squamate. It therefore collapses relationships at the base of crown squamates to a polytomy when it is included in analyses of (Extended Data Fig. 8). Analyses of our Dataset 2 place *Scandensia* as the sister taxon of *Hongshanxi*, forming a stem squamate clade that is crownward to *Bellairsia*+*Oculudentavis* (when using a molecular backbone constraint for relationships within Squamata; Extended Data Fig. 9), or in a polytomy at the base of the squamate crown (not using a molecular backbone constraint for relationships within Squamata; Extended Data Fig. 10).

The Late Jurassic (Tithonian) species *Ardeosaurus brevipes* was included in our analyses, but its position is unstable. Although many early researchers placed *Ardeosaurus* as a gekkotan[57], others have considered it to be scincoid[40]. It was placed in a polytomy at the base of the squamate crown in our main analysis (analysis of Dataset 1 with molecular backbone constraint, excluding taxa with unstable phylogenetic positions; Extended Data Fig. 7B), with very weak support for *Ardeosaurus* as the sister to *Eichstaettisaurus*+*Dibamus*+Gekkota that is shown only when displaying nodes with posterior probabilities less than 0.5 (Extended Data Fig. 7A). A similar position is also supported when relationships within the squamate crown group are not constrained the a molecular backbone (Extended Data Fig. 8B). Our analyses of Dataset 2 find *Ardeosaurus* as a stem scincoid (when using a molecular backbone constraint; Extended Data Fig. 9) or in a polytomy with Scincoidea and Lacertoidea (when not constraining relationships within Squamata; Extended Data Fig. 10). More information on the palate, braincase and vertebral column (e.g., it is uncertain whether the centra are pro- or amphicoelous) might improve resolution of the affinities of *Ardeosaurus*.

There are similar problems with two other late Jurassic (Tithonian) taxa, *Bavarisaurus macrodactylus* and *Eichstaettisaurus schroederi*, both of which were also considered gekkotan by earlier researchers[57]. *Eichstaettisaurus schroederi* is preserved in dorsal view, thereby obscuring the vertebral centra. It was placed on the gekkotan or gekkotan/dibamid stem in all of our analyses, a position consistent with previous studies. *Bavarisaurus* is more problematic as the skull of the holotype is largely represented by an impression of the dorsal and lateral surface of the skull yielding limited comparative data other than an apparently single frontal, paired premaxillae, a complete postorbital bar, a 'typically' squamate suspensorium (slender hooked squamosal, supratemporal), incomplete lower temporal bar, and possibly paired parietals. The dentary teeth are slender, pleurodont and recurved. It is certainly a pan-squamatan. Given the limited cranial data, it was not included in our analysis. Unlike *Eichstaettisaurus* and *Ardeosaurus*, however, the vertebral centra are preserved in lateral view, and show that free intercentra are retained throughout the presacral column, as in stem-squamates and gekkotans. Although these intercentra somewhat obscure the joint surfaces of the centrum, it seems likely that the centra were amphicoelous in *Bavarisaurus*. There are also three distal tarsals in the hind foot, as in *Bellairsia.* A recent analysis of squamate evolution[58] placed *Bavarisaurus* as a sister taxon to *Huehuecuetzpalli* on the squamate stem, a position that is broadly compatible with our results given the different taxon sampling, and we agree with the authors of that study that *Bavarisaurus* is probably also a stem-squamate.

Various other taxa have also recently been hypothesised as early-diverging stem-squamates, including *Megachirella wachtleri* from the Middle Triassic of Italy and *Marmoretta oxoniensis* from the Middle Jurassic of the UK [14,43]. However, both taxa have also been identified as stem-lepidosaurs in both older and more recent works, including updated phylogenetic analysis, and re-study of the most complete specimen of *Marmoretta* [22–24,59–61]. We find *Marmoretta* and *Megachirella* in a clade that lies just outside of Lepidosauria, together with *Fraxinisaura rozynekae a*nd *Paliguana whitei*. Although the lepidosauromorph affinities of these four taxa are well-supported in our analysis (pp = 0.98), the node excluding them from Lepidosauria is relatively less well-supported (pp = 0.77), meaning that either new discoveries, or more complete knowledge of the anatomy of existing specimens, may help to further evaluate their affinities, with potential implications for understanding evolutionary transformations and ancestral morphology at the base of Lepidosauria.

Our analyses also have implications for other taxa that have been proposed as stem lepidosaurs: the Triassic taxa *Vellbergia bartholomaei*[42] and *Taytalura alcoberi*[43]. *Vellbergia*, when included in analyses, has an uncertain phylogenetic position that collapses relationship of stem lepidosaurs + Rhynchocephalia + Squamata to a polytomy (Extended Data Fig. 8), it was therefore removed for our main analyses. Nevertheless, its inclusion does not alter the placement of *Bellairsia* or the other stem-squamate taxa under discussion. *Taytalura*, which was reported as a stem lepidosaur by [43], was consistently found as a non-lepidosauromorph diapsid (Extended Data Figs 7–8), which may be attributed to relatively poor preservation and a lack of definitive synapomorphies shared with other lepidosauromorphs.

Part 4. Supplementary references

51. McKerrow, W. S., Johnson, R. T. & Jakobson, M. E. Palaeoecological studies in the Great Oolite at Kirtlington, Oxfordshire. *Palaeontology* **12**, 56–83 (1969).

52. Evans, S. *et al*. The Middle Jurassic vertebrate assemblage of Skye, Scotland. In: *Proceedings of the Ninth Symposium on Mesozoic Terrestrial Ecosystems and Biota* (eds. Barrett, P. & Evans, S.) 36–39 (Natural History Museum, London, 2006).

53. Evans, S. E. The skull of a new eosuchian reptile from the Lower Jurassic of south Wales. *Zool. J. Linn. Soc.* **70**, 203–264 (1980).

54. Russell, A. P. & Bauer, A. M. The appendicular locomotor apparatus of *Sphenodon* and normal-limbed squamates. *Biol. Reptil.* **21**, 1–465 (2008).

55. Fabrezi, M., Abdala, V. & Oliver, M. I. M. Developmental basis of limb homology in lizards. *Anat. Rec.* **290**, 900–912 (2007).

56. Bolet, A. & Evans, S. E. New material of the enigmatic *Scandensia*, and Early Cretaceous lizard from the Iberian Peninsula. *Spec. Pap. Palaeont.* **86**, 99-108 (2011).

57. Hoffstetter, R. Les Sauria du Jurassique supérieur et specialement les Gekkota de Bavière et de Mandchourie. *Senck. Biol.* **45**, 281-324 (1964).

58. Bolet, A., Stubbs, T. L., Herrera-Flores, J. A., & Benton, M. J. The Jurassic rise of squamates as supported by lepidosaur disparity and evolutionary rates. eLife: 35502582 (2022).

59. Evans, S. E. A new lizard-like reptile (Diapsida: Lepidosauromorpha) from the Middle Jurassic of England. *Zool. J. Linn. Soc.* **103**, 391–412 (1991).

60. Renesto, S. & Posenato, R. A new lepidosauromorph reptile from the Middle Triassic of the Dolomites (Northern Italy). 463–474 (2003).

61. Renesto, S. & Bernardi, M. Redescription and phylogenetic relationships of *Megachirella wachtleri* Renesto et Posenato, 2003 (Reptilia, Diapsida). *Palaontologische Zeitschrift* **88**, 197–210 (2014).

Part 5. List of synapomorphies of particular clades:

Lepidosauromorpha

42. Quadratojugal foramen: absent (0)/ **present (1)**

67. Frontals, fusion to each other: unfused (0)/ **fused (1)**

68. Frontals, parietal tabs: absent (0)/ **present (1)**

167. Dentaries, anterior end, split by Meckelian canal: absent (0)/ **present (1)**

219. Atlas, neural arches, postzygapophyses: absent (0)/ **present (1)**

235. Intercentra, on cervical vertebrae: absent (0)/ **present (1)**

237. Intercentra, on dorsal vertebrae: absent (0)/ **present (1)**

302. Ischia, ischiadic tuberosity: absent (0)/ **present (1)**

307. Humeri, entepicondyle foramen: absent (0)/ **present (1)**

312. Humeri, secondary ossification of epiphyses: absent (0)/ **present (1)**

349. Angular lateral exposure: exposed along 1/3 of the lateral face of the mandible (0)/ **exposed only as a small sliver along the lateral face (1)**

350. Maxilla orbital exposure: absent (0)/ **present (1)**

352. Frontal morphology: parallelogram shaped (0)/ **hour-glass shaped (1)**

358. Lacrimal size: large, with an anterior or posterior (suborbital) process which is longer anteroposteriorly than the dorsoventral length of the lacrimal in lateral view (0)/ **small, dorsoventral length greater than anteroposterior length confined to the orbital rim (1)**

368. Penultimate phalanges in hand: shorter than or equal to antepenultimate (0)/ **longer than antepenultimate (1)**

369. Jugals, posteroventral process: **short or spur-like, anteroventrally less than 20% of the total ventral length (0)** / long, greater than 25% of the total ventral length (1)

376. Posterior dentary teeth, interdental plates: contact both labial and lingual walls of alveolar groove, fully separating adjacent teeth (0)/ **do not contact both labial and lingual walls of alveolar groove or are absent (1)**

377. Posterior dentary teeth, asymmetry of dorsoventral height of labial and lingual walls of alveolar groove: lingual wall subequal in height to labial wall (0)/ **lingual wall absent or low, less than half the height of the labial wall (1)**

379. Posterior maxillary teeth, interdental plates: contact both labial and lingual walls of alveolar groove, fully separating adjacent teeth (0)/ **do not contact both labial and lingual walls of alveolar groove or are absent (1)**

380. Posterior maxillary teeth, asymmetry of dorsoventral height of labial and lingual walls of alveolar groove: lingual wall subequal in height to labial wall (0)/ **lingual wall absent or low, less than half the height of the labial wall (1)**

(*Paliguana*, *Megachirella*, *Fraxinisaura+Marmoretta*)

81. Parietals, ventral side, parietal fossa: **present (0)**/ absent (1) [? in *Megachirella*, *Fraxinisaura*]

140. Prootics, prootic crest: **absent (0)**/ present (1) [? in *Marmoretta*, *Fraxinisaura*]

189. Articulars, foramen chorda tympani: **absent (0)**/ present (1) [? in *Paliguana*, *Fraxinisaura*]

200. Coronoids, posterodorsomedial process: **present (0)**/ absent (1) [? in *Paliguana*, *Fraxinisaura*]

(Rhynchocephalia, Pan-Squamata, *Sophineta*)

69. Frontals, subolfactory processes: absent (0)/ **present (1)**

118. Quadrate foramen: **present (0)**/ absent (1)

121. Quadrates, quadrate conch: absent (0)/ **present (1)**

217. Atlas, pleurocentrum, fusion to axis: unfused (0)/ **fused (1)**

227. Presacral pleurocentra, notochord, persistent in adults: **present (0)**/ absent (1)

229. Presacral pleurocentra, midventral crest, cervical vertebrae: absent (0)/ **present (1)**

296. Ilia, anterior pubic process: absent (0)/ **present (1)**

Rhynchocephalia

55. Squamosal, anterior process, dorsoventral length: narrow, < one-quarter of the dorsoventral length of the postorbital region (0) /**deep, > one-third of the dorsoventral length of the postorbital region (1)**

59. Postfrontals, medial margin, position, relative to parietal: ventral (0)/ **dorsal (1)**/ lateral (2)/ anterior (3)

111. Pterygoids, arcuate flange: absent (0)/ **present (1)**

173. Dentaries, coronoid process, dorsal expansion: absent (0)/ **present (1)**

176. Splenials: **absent (0)**/ present (1)

182. Surangulars, coronoid process: absent (0)/ **present (1)**

360. Lateral row of enlarged palatine teeth: absent (0)/ **lateral tooth row present on palatine, converging posteriorly (1)**

361. Dentaries, posterior extent: extends posteriorly no further than the level of coronoid eminence or slightly beyond (0)/ **extends posteriorly more than halfway between coronoid eminence and articular condyle (1)**

Pan-Squamata (reversals and missing data in taxa higher on the tree than Gekkota not indicated)

38. Quadratojugals: present (0)/ **absent (1)**

51. Squamosals, dorsal process: **absent (0)**/ present (1)

68. Frontals, parietal tabs: **absent (0)**/ present (1)

72. Parietals, fusion: unfused (0)/ **fused (1)**

89. Vomers, teeth: **absent (0)**/ present (1)

91. Vomers, lateral expansion: absent (0)/ **present (1)**

95. Vomers, shape in cross-section: flat (0)/ **convex ventrally (1)**

97. Palatines, teeth: **absent (0)**/ present (1)

116. Epipterygoid, base shape: base flared out (0)/ **base columnar, inserting into a pit on the surface**

of the pterygoid (1)

119. Quadrates, pterygoid process: present as broad, overlapping quadrate/pterygoid suture (0)/

absent or reduced to a small lappet on the ventromedial surface of the quadrate (1)

123. Quadrates, cephalic condyle, notch for the squamosal: absent (0)/ **present (1)**

124. Carotid foramina, entrance in braincase, position: **lateral wall of braincase (0)**/ ventral

surface of braincase (1)

126. Supraoccipital, medial ascending process: absent (0)/ **present (1)**

135. Basisphenoid, Vidian canal: open (0)/ **fully enclosed (1)**

153. Exoccipitals, crista tuberalis: absent (0)/ **present (1)**

282. Procoracoid, coracoid emargination: absent (0)/ **anterior emargination (1)**/ anterior and posterior emarginations (2)

286. Clavicles, proximoventral fenestration: absent (0)/ **present (1)**

340. Gastralia: **absent (0)**/ present (1)

350. Maxilla orbital exposure: **absent (0)**/ present (1)

354. Orientation of transverse flange of pterygoid: directed predominantly laterally or posterolaterally (0)/ **oriented in an anterolateral direction (1)**

365. Jugal, anterior suborbital extension: broadly separated from prefrontal or posterior to the midpoint of the orbit (0)/ **reaches level of prefrontal or anterior margin of orbit (1)**

367. Jugal lateral exposure below orbit: absent (0); partly exposed above orbital margin of maxilla (1)/ **entirely exposed above orbital margin of maxilla (2)**

382. Metotic fissure: undivided (0)/ **subdivided (1)**

Bellairsia+(*Huehuecuetzpalli*+*Oculudentavis*)

59. Postfrontals, medial margin, position, relative to parietal: ventral (0)/ dorsal (1)/ lateral (2)/ **anterior (3)**

73. Pineal foramen: present (0)/ **absent (1)** [in adults of *Huehuecuetzpalli*]

79. Parietals, nuchal fossa: absent (0)/ **present (1)** [? in *Oculudentavis*]

102. Palatine foramen: absent (0)/ **present (1)** [? in *Huehuecuetzpalli*]

110. Pterygoids, main body, concave in ventral aspect: absent (0)/ **present (1)** [? in *Huehuecuetzpalli*]

208. Posterior dentition, replacement teeth, position in relation to functional teeth: lingual (0)/ **posterolingual (1)** [? in *Huehuecuetzpalli*]

274. Scapula, supraglenoid buttress: absent (0)/ **present (1)** [? in *Huehuecuetzpalli*]

Huehuecuetzpalli+Oculudentavis

33. Prefrontal crest: absent (0)/ **present (1)**

60. Postfrontals, parietal process: **absent (0)**/ present (1)

348. Postfrontal contribution to upper temporal fenestra: **postfrontal excluded (0)**/ postfrontal included (1)

Squamata without (*Bellairsia+*(*Huehuecuetzpalli+Oculudentavis*))

125. Supraoccipital, lateral ascending processes: absent (0)/ **present (1)**

138. Basisphenoid (or fused parabasisphenoid), ventral aspect, shape, concavity: single (0)/
divided (1)/ **absent (2)**

226. Presacral pleurocentra, orientation of centrum: amphicoelous (0)/ **procoelous (1)**/opistocoelous (2)/ platycoelous (3)/ amphyplatyan (4)

227. Presacral pleurocentra, notochord, persistent in adults: present (0)/ **absent (1)**

246. Neural arches, presacral vertebrae, zygosphenes: absent (0)/ **present (1)**

291. Interclavicle, anterior process: absent (0)/ **present (1)**

307. Humeri, entepicondyle foramen: **absent (0)**/ present (1)

314. Radia, distal epiphysis, styloid process: absent (0)/ **present (1)**

317. Ulnae, distal epiphysis, expansion: absent (0)/ **present (1)**

328. Tibiae, distal epiphysis, notch: absent (0)/ **present (1)**

346. Skull proportions: preorbital skull length equal to postorbital length (0); preorbital length exceeds postorbital skull length (1)/ **postorbital length exceeds preorbital skull length (2)**

347. Prefrontal/palatine antorbital contact: absent (0); narrow forming less than 1/3 the transverse distance between the orbits (1)/ **contact broad, forming at least 1/2 the distance between the orbits (2)**

355. Humeral torsion: proximal and distal end are off-set at an angle of at least 45°(0)/ **off set is reduced to no more than 20° (1)**